FABRIC-REINFORCED, CEMENT-BASED LAMINATED COMPOSITES:

AN EXPERIMENTAL AND THEORETICAL STUDY

by

Jitendra Pahilajani

A Thesis Presented in Partial Fulfillment
of the Requirements for the Degree
Master of Science

ARIZONA STATE UNIVERSITY

July 2004

FABRIC-REINFORCED, CEMENT-BASED LAMINATED COMPOSITES:

AN EXPERIMENTAL AND THEORETICAL STUDY

by

Jitendra Pahilajani

has been approved

July 2004

APPROVED:

_____, Chair

_____

_____

_____

Supervisory Committee

ACCEPTED:

_____

Department Chair

_____

Dean, Division of Graduate Studies

ABSTRACT

Fabric-reinforced, cement-based composites are relatively new in the field of construction. Its advantages are superior tensile strength and ductility. To check the behavior of the composites in tension, a series of tensile tests were carried out using several different fabric cement manufacturing techniques, matrix, and fabric types. There were four fabric types: alkali-resistant glass, polypropylene, polyethylene, and Polyvinyl Alcohol; two different mix designs (control and with flyash); and two different manufacturing procedures: pultrusion and cast.

The damage evolution in fabric-cement composites under tensile loading was studied as a function of the applied strain. Three distinct measures of damage are evaluated and include quantitative crack spacing by image analysis, stiffness degradation, and micro-structural evaluation by optical and scanning electron microscopy. The evolution of crack spacing as a function of applied strain was correlated with the tensile response as well as with the stiffness degradation. It was observed that the mechanical properties along with crack spacing and composite stiffness were significantly affected by the matrix formulation, curing procedure, and the intensity of the pressure applied after the pultrusion process. The best tensile performance was achieved for glass fabric composites with a high content of flyash.

Further study was therefore carried on the properties of flyash composites. This involved development of a relationship between the mix constituents, rheology tests, and the mechanical properties. Various flyash contents ranging from 0 to 80% replacement by volume of the cement were studied in composites reinforced with AR glass fabrics. The rheological properties of the fresh matrix were examined and correlated with the

mechanical performance. Results indicate an improvement in the mechanical behavior of the cement composite with flyash compared to similar composites without flyash. A good correlation was found between the rheology properties of the fresh mixture and the mechanical performance of the composite.

The last objective was to theoretically model the tensile behavior of these systems. The results of the crack spacing and stiffness degradation studies were incorporated in the model. It was checked for various systems of mix designs and fabric types. The model simulated similar trends to those of experimental results.

….To My Parents

ACKNOWLEDGEMENTS

I express my sincere gratitude to my advisor and committee chair, Dr. Barzin Mobasher, for his constant guidance, support and help throughout the course of the study. I would also like to extend sincere gratitude to Dr. Subramaniam D. Rajan who inspired me to learn FEM and other programming tools which are going to be invaluable. Thanks also to Dr. Kamil Kaloush for his encouragement throughout my MS degree and for being on my committee. I also extend my thanks to Dr. Alva Peled for her guidance and help for the extensive summer experiments and her continuous help on many papers and other research work. I am indebted towards Dr. Robert Hinks who has helped me grow as person when I worked under him as teaching assistant. I greatly appreciate the help provided by Dr. Dallas Kingsbury and Peter Goguen in day to day laboratory work. Without them my task would have been very difficult. Thanks are also extended to my laboratory mates, Sachiko Sueki and Dnyanesh Naik for helping me in research. I am very glad to have moral boosting friends like Nora Singla , Himanshu Joshi, Amit Sankhe, Vivek Sharma, Satish Sadhu and Agrawal Navneet who have always been there at the time of my need. I am grateful to Rimpal and Gautham who helped me gel into the MS program and research work with ease. Finally, I would like to acknowledge all my friends, especially Srihari, Paul and Satish for their constant support. I would also like to express my gratitude to all the CEE administrative staffs and folks at International Student Office for their kind help and support. Last and the most important I would like to thank my mother, Mona Pahilajani and father Khushal Pahilajani whose blessings and sacrifice have brought me to this place along with the love from my younger sister Neha.

TABLE OF CONTENTS

Page

LIST OF TABLES ix

LIST OF FIGURES x

CHAPTER

1 INTRODUCTION 1

1.1 Introduction 1

1.2 Review of Related Literature 4

1.3 Objectives of the Thesis 5

2 EXPERIMENTAL ANALYSIS AND RESULTS 9

2.1 Tension Test 9

2.2 Sample Preparation 12

2.3 Testing 15

2.4 Discussion of Tests results 15

2.5 Microstructure 28

3 FLYASH BASED COMPOSITES 34

3.1 Experimental 34

3.2 Testing 36

3.3 Discussion of Tests results 37

3.4 Rheology 45

3.5 Microstructure 49

CHAPTER Page

4 CRACK SPACING MEASUREMENT AND STIFFNESS DEGRADATION 50

4.1 Crack Spacing Measurements.. 51

4.2 Measurement of the stiffness degradation from the stress-strain plots 57

5 THEORETICAL MODEL 60

5.1 Nonlinear Stress Strain Response.. 60

5.2 Crack Spacing Evolution Law 64

5.3 Theoretical Simulation of Fabric Pullout 66

5.4 Formulation for a Singla Lamina 68

6 CONCLUSION 84

REFERENCES 88

APPENDIX

A GRAPHS FOR ALL THE TESTED SAMPLES (7 Days)..... 91

B GRAPHS FOR ALL THE TESTED SAMPLES (28 Days)..... 96

C GRAPHS FOR COMPARISONS..... 100

LIST OF TABLES

Table		Page
2.1	Properties of Yarns	10
2.2	Mix Design Detail	12
2.3	Average tensile properties of the different pultruded specimens, exposed to accelerate curing	27
3.1	The Mix Design (by volume) used in the study	35
3.2	Average Mechanical Properties of samples from each group (7 and 28 day curing period) along with the standard deviation values	40
3.3	Yield Strength and Viscosity values for the four mix designs	47
4.1	Calibration readings	54
4.2	Crack Spacing parameters with respect to strain	56
4.3	Stiffness degradation constants for different specimen types	59
5.1	Different Mix Properties	63
5.2	Experimentally measured properties	64
5.3	Experimentally measured properties (continued)	64
5.4	Various Crack Spacing parameters used in the theoretical model	66

LIST OF FIGURES

Figure		Page
2.1	Fabric types	11
2.2	Schematic of the pultrusion set up	13
2.3	Manufacturing of fabric cement composites with the pultrusion process	14
2.4	Load Displacement plot for a single layer of fabric tested in tension	16
2.5	Stress Strain plot of composites tested in tension	17
2.6	Comparison of glass and PE fabrics composites: (a) tensile stress and crack spacing vs. strain, (b) tangent stiffness vs. crack spacing	19
2.7	Effect of curing (a) tensile stress and crack spacing vs. strain, (b) tangent stiffness vs. crack spacing, of glass fabric composites with addition of fly ash	24
2.8	Effect of the pressure apply after the pultrusion process: (a) tensile stress and crack spacing vs. strain, (b) tangent stiffness vs. crack spacing	26
2.9	Crack propagation in pultruded glass fabric composite: (a & b) crack propagation across the loading direction, (c) cracking across and along the loading direction at failure	29
2.10	(a & b) Crack propagation across the loading direction of woven PE fabric cement composite and (c) schematic description of the stresses developed at the fabric junction	30
2.11	Failure of the fabric at the end of testing in glass-fabric composite	31

Figure Page

2.12 SEM micrographs of the fabric in pultruded cement composite with high content of silica fume (10%): (a) glass yarn along the pultruded direction, (b) PE fabric at the junction of the yarns, (c) glass yarn perpandicular to the pultrusion direction..... 32

2.13 SEM micrographs of fabric embeded in cement composite with different content of superplastisizer: (a) high content (matrix #3 in Table 2.1) and (b) with low content (matrix #1 Table 2.1) 33

3.1 The bonded AR Glass Fabric Mesh..... 36

3.2 Tensile Stress Strain plot of samples with 60% fly ash content 41

3.3 Comparison of the tensile stress strain response of samples with 40% fly ash content at 7 and 28 days 41

3.4 Comparison of stress strain response of specimens with different fly ash contents and control sample (a) after 7 days (b) after 28 days 42

3.5 Showing the Crack Spacing Characteristics along with the Stress strain of samples at 7 and 28 days 43

3.6 Stress strain response after 28 days accelerated ageing compared with control samples 44

3.7 Shear strength vs. shear rate plots for various levels of flyash 46

3.8 Shear strength vs. shear rate plots for various levels of flyash with 5% Silica Fume 48

Figure Page

3.9 Shear strength vs. shear rate plots for various levels of flyash with 10% Silica Fume 48

3.10 a) Fly ash (60% mixture) in the vicinity of the yarn junction b) The matrix penetration in between the two adjacent fabric layers (60% mixture). 49

4.1 Image analysis procedure: (a) & (b) images of specimens during tensile tests, (c) trace lines of cracks, (d) vertical lines for distribution of crack spacing 52

4.2 Photograph used for calibration 53

4.3 Typical Crack Spacing Curve for a sample with AR Glass and 40% flyash 55

4.4 Typical Stiffness degradation plot along with the crack spacing evaluation for a sample with AR glass and no super-plasticizer 58

5.1 Stress strain and the crack spacing response of AR Glass fabric reinforced cement based composite 61

5.2 Glass Sample (a) At 0.9% strain (b) At 2.5% strain 62

5.3 Definition of lamina and coordinates used in generating stiffness coefficients 68

5.4 Parametric study for glass and polyethylene systems 72

5.5 Graph showing the behavior of the model with varying volume fraction 77

Figure Page

5.6 Graph showing the behavior of the model with varying stiffness values of the AR Glass fabric 77

5.7 Graph showing the behavior of the model with varying values of bond strength of the AR Glass fabric 78

5.8 Stress and crack spacing plots plotted versus strain for a sample with glass fabric (40% flyash) along with the theoretical model response which gives the fit for the crack spacing and the stress strain response 79

5.9 Stress and crack spacing plots plotted versus strain for 2 samples with poly-ethylene fabric along with the theoretical model response which gives the fit for the crack spacing and the stress strain response 80

5.10 Stress and crack spacing plots plotted versus strain for samples with glass fabric (with and without flyash) along with the theoretical model 81

5.11 SEM image of sample with 40% flyash showing the flyash particles: (a) occupying the voids (b) covering the surface of the fabric even after failure 82

5.12 Stress and crack spacing plots plotted versus strain for samples with glass fabric (with and without pressure) along with the theoretical model 83

Figure Page

A-1 AR-glass fiber samples with matrix #5 (7 days) 92

A-2 AR-glass fiber samples with matrix #2 (7 days) 92

A-3 AR-glass fiber samples with 40% Flyash content and 5% Silica Fume (7 days)..... 93

A-4 AR-glass fiber samples with 80% Flyash content and 5% Silica Fume (7 days)..... 93

A-5 PE fiber samples with matrix #2 (7 days) 94

A-6 PE fiber samples with 60% Flyash content and 5% Silica Fume (7 days)... 94

A-7 PE fiber samples with 60% Flyash content (7 days) 95

A-8 PP fiber samples with Matrix#2 and cast in opposite direction of fabric (7 days) 95

B-1 AR-glass fiber samples with matrix #5 (28 days) 97

B-2 AR-glass fiber samples with matrix #2 (28 days) 97

B-3 AR-glass fiber samples with 40% Flyash content and 5% Silica Fume (28 days) 98

B-4 AR-glass fiber samples with 60% Flyash content and 5% Silica Fume (28 days) 98

B-5 AR-glass fiber samples with 80% Flyash content and 5% Silica Fume (28 days) 99

B-6 PE fiber samples with matrix #2 (28 days) 99

C-1 Comparison of AR-glass fiber samples with matrix #5 at 7 and 28 days 101

Figure Page

C-2 Comparison of AR-glass fiber samples with matrix #2 at 7 and 28 days 101

C-3 Comparison of AR-glass fiber samples with 40% Flyash at 7 and 28 days 102

C-4 Comparison of AR-glass fiber samples with 60% Flyash at 7 and 28 days 102

C-5 Comparison of AR-glass fiber samples with 80% Flyash at 7 and 28 days 103

C-6 Comparison of PE fiber samples with matrix#2 at 7 and 28 days 103

C-7 Comparison of AR-glass fiber samples with 40% FA and 0% FA (5% SF) 104

C-8 Comparison of AR-glass fiber samples with 60% FA and 0% FA (5% SF) 104

C-9 Comparison of AR-glass fiber samples with 80% FA and 0% FA (5% SF) 105

C-10 Comparison of AR-glass fiber samples with 40% FA and 0% FA (No SF) 105

C-11 Comparison of AR-glass fiber samples with 6% FA and 0% FA (No SF) 106

C-12 Comparison of AR-glass fiber samples with 80% FA and 0% FA (No SF) 106

Figure Page

C-13 Comparison of AR-glass fiber samples with fabric in 0 and 90 orientations 107

C-14 Comparison of PP fiber samples with fabric in 0 and 90 orientations 107

CHAPTER 1

INTRODUCTION

1.1 Introduction

Researchers are always thriving to improve the quality of various materials used in the industry. The growing demand in the market is for materials that are durable, strong, easily available and most importantly less expensive as compared to the conventional methods. Composite materials are nowadays extensively studied so as to increase its use and also check the strength and safety aspects that are involved with any new material. The basic definition of a composite material is:

a. It consists of two or more physically distinct and mechanically separable materials.
b. It can be made by mixing the separate materials in such a way that the dispersion of one material in the other can be done in a controlled way to achieve optimum properties.
c. The properties are superior, and possibly unique in some specific respects, to the properties of the individual components.

Examples of naturally occurring composites materials are wood and bone. Manmade composites probably began with the addition of straw to mud or clay to create reinforced building materials. A very common structural composite is concrete, which uses rocks to reinforce cement. Reinforced concrete uses both rocks and steel rods for reinforcement, where the steel serves mainly to support tensile loads. In all these

examples, properties of composites are different from, but depend on, the properties of the constituent materials.

Although reinforcements can take various shapes, the presentation of composites in this work is entirely on fabric reinforced materials. Fibers are utilized for their high strength and/or stiffness. The small dimension of a fiber minimizes the presence of significant flaws in a brittle material such as glass, allowing the fiber strength to approach the material's theoretical strength.

Fabrics are not directly usable alone and must be combined with a matrix material, which performs the following functions:

a) Binds fibers together.

b) Transfers loads to the fibers

c) Protects fibers from damage

The matrix in this study consists primarily of cement and water. Variations in the matrix are obtained by addition of pozzolannic materials like Silica Fume and Flyash to study their effects on the composite system.

Fibers can be

1. Continuous – long, continuous fibers, which either run in a single direction in a single sheet of uniform thickness, or are woven into a fabric. In either case, the fiber lengths are on the order of the outside dimensions of the part.
2. Discontinuous – random or oriented, as in molded plastics.

A single layer of unidirectional composite is generally not useful because of very low strength transverse to the fibers. Therefore, laminae (layers or plies) are combined with their fibers oriented in more than one direction to form a laminate.

The wide variety of fibers and matrix materials available today has resulted to a large extent from their applications in aerospace structures. But nowadays the concept of composites and use of fabrics is gaining popularity in the field of structural engineering. Various laboratories and materials scientist are studying different combinations of matrix and fabric type to help in establishing a new genre of material in this field. As the application of fiber composites will grow, the cost of raw materials will decrease, and thus the task to develop new manufacturing techniques will gain importance.

The reason for using fibers in composite is to enhance the properties of an inherently weak, brittle and crack-prone cementitious matrix. Fiber in hardened cement paste, mortar or concrete may have at least three important effects. First, they may tend to increase the stress at which the matrix starts to crack. Second, they may improve the strain capacity or ductility of the inherently brittle cementitious matrix, thus increasing its energy absorption capability or toughness characterized in general by the area under a stress-strain or load-deformation curve or some defined portion of it. A third important effect of fibers is their tendency to inhibit or modify crack development in terms of reducing crack width and average crack spacing. The degree of improvements depends on the mode of loading and the type and amount of fibers. Any type of fiber effective for reinforcing relatively weak and brittle cementitious matrices must have higher tensile strength, ductility (or elongation), elastic modulus, elasticity and Poisson's ratio than

those of matrix. However, realization of full reinforcing potential depends strongly on the interfacial shear bond between fiber and matrix.

In the simplest case of very long fibers aligned in the direction of uniaxial tensile stress, just like conventional straight reinforcing bars, it should be obvious that if adhesive interfacial shear bond does not exist, no tensile stress can develop in the fibers. In this case the strength of the composite is the same as the strength of the matrix because the fibers pull out of the matrix without resistance. In contrast, when there is very strong interfacial shear, whether by adhesion, friction or mechanical interlock, the fibers become subject to the entire load carried by the composite once the matrix cracks, and the ultimate strength depends only on the amount and intrinsic strength of the fibers. However, if the toughness of the composite was concerned, the interface must not be so strong that it does not fail and allow toughening mechanisms such as debonding and fiber pullout to take place.

1.2 Literature review

There is a growing interest in the use of fabrics as reinforcement for cement components. Several researchers Swamy & Hussin (1990), Perez-Pena (1991), Peled (1998), Peled & Bentur (2000), Kruger (2003), and Meyer & Vilkner (2003) reported the high potential for use of cement-based products reinforced with fabrics. In addition to ease of manufacturing, fabrics provide benefits such as excellent anchorage and bond development. The mechanical anchoring is provided by the non-linear geometry of individual yarns within the fabric, induced by the fabric structure Bentur (1997) and Peled [1998]. The fabric structure induces turtuosity in the path of propagation of a crack

promoting crack deflection processes that lead to the enhanced strength of the composite. Another important parameter is the effectiveness of fabric embedment in a matrix of cement paste. The matrix penetration through the openings in fabric microstructure contributes to the anchorage and increases the ability of the yarns to carry the load. The geometry of the fabric is thus responsible for transfer of the load between the matrix and the fibers, significantly reducing the dependence on the interface transition zone and processes such as debonding and pullout which normally serve as load transfer mechanism. Therefore, the use of fabrics for cement products requires optimization of fabric structure and the resulting geometry of the yarns in the fabric, in addition to an improvement in the understanding of underlying toughening mechanisms.

An efficient production method for fabric-cement composites is the pultrusion process. Earlier studies showed that cement composites containing 5% (AR) unidirectional glass fibers produced by pultrusion achieved tensile strength of 50 MPa Mobasher, Pivacek and Haupt (1997), compared to an average tensile strength of about 6-10 MPa of conventional GFRC (Glass Fiber Reinforced Cement) composites. Recently a pultrusion based method to produce fabric-cement composite was developed and preliminary results are discussed in a recent publication Peled and Mobasher (2003).

1.3 Objective of the thesis

The behavior of fabric-cement composites exposed to tensile loads is characterized by multiple cracking. These distributed transverse cracks form gradually as the composite is loaded beyond the initial cracking stages. The nature of multiple cracking and the resulting stress-strain curve, toughness, and strength, are dependent on

the properties of the reinforcing fabrics, the cement matrix, as well as the interface bond developed. Therefore, parameters which lead to crack formation ultimately control the fabric-cement composite properties. Microstructural features such as crack spacing, width, and density allow formulation of the damage evolution as a function of macroscopically applied strain. This can help in correlating various fabric types and mixture formulations with increases in modulus of rupture, ductility, and increased strain capacity of different composites. The composite stiffness in the post crack range is an important property that should be considered. A general relationship between the crack spacing and the stiffness at various stages of loading can be compared with the damage development as the strain increases.

Composites with low modulus polyethylene woven fabric, bonded glass mesh, polypropylene and PVA (Poly Vinyl Alcohol) fabrics were manufactured by means of the pultrusion technique. In order to optimize the development of composites, several factors such as the fabric type and structure, matrix formulation, and the processing parameters are addressed.

An important objective of this study was to see the effect of changing the matrix by additives like flyash. Use of flyash is becoming more and more popular in construction and the effect of this pozzolannic material on the fabric system needs to be addressed. The fabric mainly used here is AR glass and flyash levels used are 40, 60, and 80 percent by weight replacement of cement. With such high levels of flyash the rheology of the mix gets affected. The workability is considerably increased. Hence to study this effect, rheological experiments were carried out and the results were analyzed. Another aspect studied was the microscopic properties of the composites after failure. For

this, scanning Electron Microscopy was carried out on samples which were cut to the size so that it could fit into the SEM. The effects of pozzolannic admixtures were further studied using the SEM images.

The third objective of the study was to develop a theoretical model for tensile tests. In order to commercially utilize new composite materials in civil engineering applications, simple and effective analysis and design guides are needed. Theoretical models are also needed to predict the response of laminated composites in order to better understand the interaction between the various phases and aid in the design of overall structural system. The present work presents a general framework for analysis and design for modeling the uniaxial response of composite laminates. The proposed methodology can be used for new composite materials or strengthening components of an existing structure. The motive here was to predict the experimentally generated results using this model so as to develop a procedure to predict responses of various fabric matrix combinations without physically making and breaking specimens.

The role of fabrics was modeled as a discrete phase. And once the lamina model was developed, the effect of fabric was homogenized and the results are presented as an effective material response. A Fabric pullout test results were used to measure the interfacial properties. The variable parameters were the embedded length, fabric sizing, and the age of the paste for the matrix. The pullout slip response was used to characterize the effect of the interface properties and age on pullout slip behavior. One of the most critical parameters is the stiffness of the fabric system due to the weave pattern and the matrix filling as it will serve to act as an important parameter of the closing pressure formulation.

An anisotropic scalar damage parameter was defined to relate to the macroscopic longitudinal strain to the reduction in crack spacing by Mobasher (1990).

A theoretical model is then developed to relate the interface bond properties to the strengthening and toughening. The toughening is modeled using the fabric pullout closing pressure formulation. The first step of simulation deals with theoretical fabric pullout response as affected by the parameters of interface and calibration of experimental pullout results.

The proposed method is based on the classical laminate theory, as we try to expand on the first order approximations that overestimate the ply discount method by Talreja (1986) and Allen (1987).

Details of the tests (experiments) are explained in Chapters 2 and 3 with chapter three dealing specifically with use of flyash. Chapter 4 discusses crack spacing study and explains the various parameters involved. Details of the theoretical model are explained in Chapter 5 and conclusions are outlined in Chapter 6.

CHAPTER 2

EXPERIMENTAL PROGRAM

2.1 Tension Test

A series of tensile test were designed to obtain the behavior of different fabric/matrix interface with respect to the strength, cracking response and the strain capacity. A combination of 4 different fabrics and 6 different mix designs, specimens were made. These specimens were subjected to three different types of curing. The curing procedures used were 7 and 28 days water curing and some of the samples after 28 days were kept into an oven to study the effect of ageing. The last type of ageing was specifically selected to understand the behavior of specimens which had flyash in them. The size of the specimens was approximately 6 inches and a width of 1 inch. The thickness of the samples varied between 0.2 to 0.6 depending upon the fabric type and the workability of the mix.

Fabric Type

Four different types of fabrics were used in the experiment, which are alkali-resistant AR-glass (AR-glass), polypropylene (PP), polyethylene (PE), and Polyvinyl Alcohol (PVA) fabrics. Fabrics are shown in figure 2.1. The properties for these fabrics are given below (Table 2.1).

Table 2.1

Properties of Yarns

Yarn Type	Yarn Nature	Strength (MPa)	E (MPa)	Strain at Peak (mm/mm)	Filament size (mm)	Number of filaments in a bundle	Approx. bundle dia. (mm)
AR-glass	Bundle	1276-2448	78600	-	0.0135	400	0.27
PP	Bundle	500	6900	0.27	0.04	100	0.40
PE	Monofilament	260	1760	0.21	0.25	1	0.25
PVA	Bundle	227	3938	0.11	-	-	0.97

Fi) PV

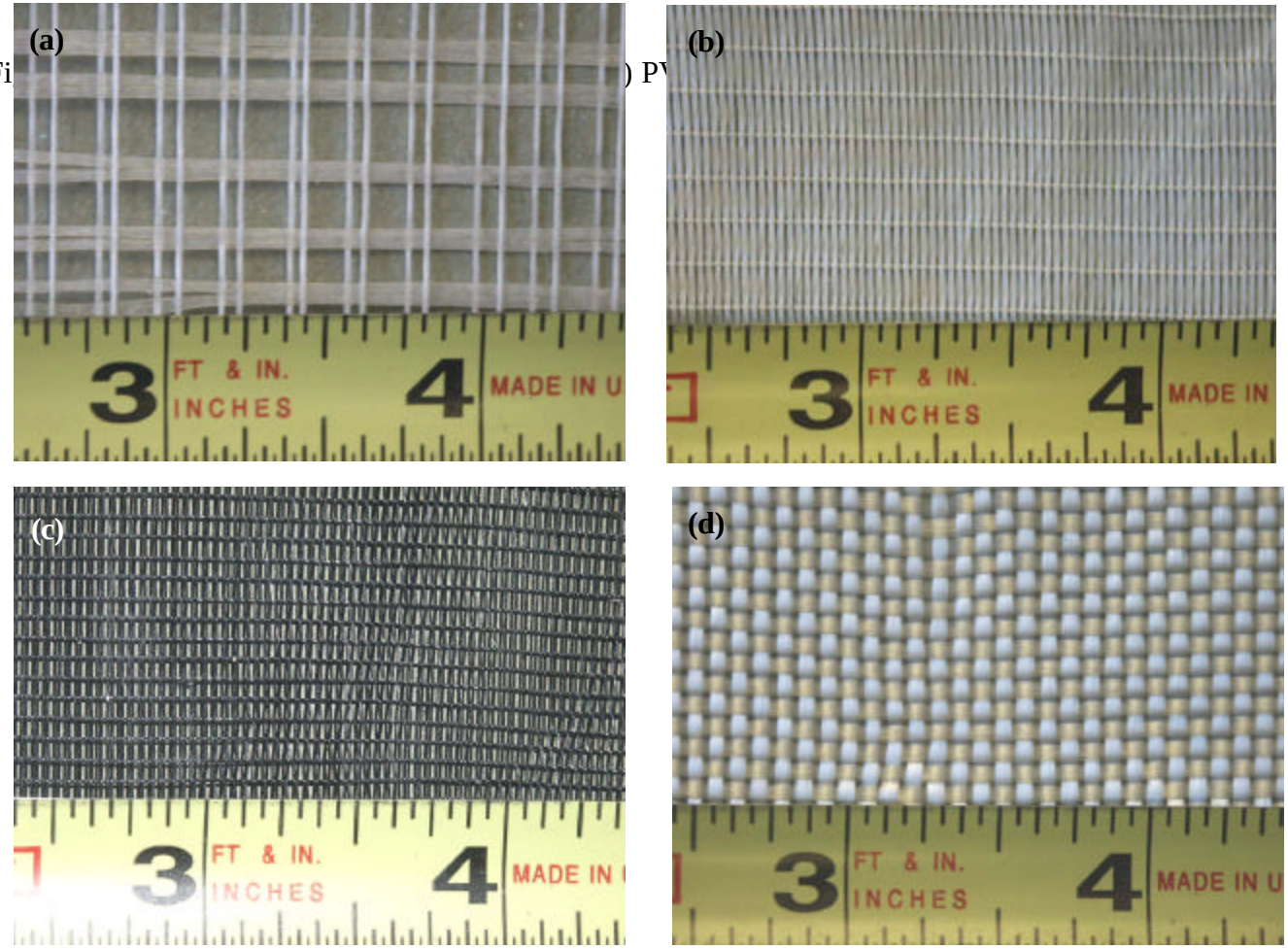
(a)
3
FT & IN.
INCHES
4
(b)
3
FT & IN.
INCHES
4
(c)
3
FT & IN.
INCHES
4
(d)
3
FT & IN.
INCHES
4

2.2 Sample Preparation

Mix Design

Controlling the rheological properties of the cement mixture is an important processing factor since the mixture should be relatively fluid to allow movement of the fabric through the cement slurry but of sufficient adhesion strength so that it will coat the fabric in the process. In order to develop a mixture with a range of porosity, rheology, and strength characteristics, two levels of silica fume and one level of fly ash were used as presented in Table 2.2. In addition, plain paste without any mineral admixture was also tested. In all cases, the water/binder ratio by weight was 0.375.

Table 2.2

Mix Design Detail

	Volume Fraction (% by weight)			
Matrix #	#1	#2	#3	#5
Cement	42	42	40	44
Silica Fume	5	5	10	---
Fly Ash	---	---	---	---
Super-plasticizer	0.1	0.2	0.4	---

Pultrusion process

Specimens were produced with the pultrusion process. A schematic drawing of the process is presented in figure 2.2 and a photograph of the setup is shown in figure 2.3.

The fabrics were passed through a slurry infiltration chamber, and then pulled through a set of rollers to squeeze the paste in the openings of the fabric, remove excessive paste, and form composite laminates on a mandrel. Fabric-cement sheets with width of 20 cm, length of 33 cm and thickness of about 1 cm were produced. Each board was made with 8 layers of fabric, yielding a reinforcement content of about 4.5%, and 9.5% by volume of AR glass, and PE fabric, respectively. After forming the sample, pressure was applied on top of the laminates to improve interlaminar bonding and penetration of the matrix in between fabric opening. A constant pressure of 15.3 KPa was applied on the surface of the fabric-cement sheet. Most of this pressure was removed 1 hour after casting, with only a 1.7 KPa stress maintained up to 24 hours from the pultrusion process. Effect of pressure applied after casting was one of the variables studied.

Fig. 2.2. Schematic of the pultrusion set up.

Fig. 2.3. Manufacturing of fabric cement composites with the pultrusion process

Curing

The panels were cut to dimensions of 25x180x12 mm within 24±1 hours after casting. Three types of curing were used. In the accelerated curing approach, specimens were cured for 3 days in 80ºC steam and then stored in room environment until testing on 7 days after the pultrusion process. In the regular curing approach, specimens were cured in 100% Relative Humidity (RH) for 25 days and then stored in room environment until testing at the age of 28 days. The third type of curing was done to see the behavior of the samples when subjected to ageing. This was achieved by removing some of the samples from the 28 day curing chamber and keeping them further for 28 days in an ageing chamber which was set at a temperature of 80^{o}C. At least 4 specimens were examined at each level of curing and the average results of the samples are reported.

2.3 Testing

Mechanical Performance - Test Methods

Closed loop control direct tensile tests were performed on both AR-Glass and Polyethylene fabric composites using a MTS testing machine with a capacity of 89KN. Metal plates with dimension of 25x30 mm were glued on the surface of the specimen at the grips to minimize damage. The tensile load and elongation were recorded and converted to stress-strain response. Photographs were taken of the samples at fixed time intervals to measure the crack formation. The tensile strength, stiffness, ductility, strain capacity, and cracking parameters were measured. The stress strain graph was used to calculate the tangent stiffness at several designated strain levels. Results were used to correlate the stiffness degradation with crack spacing data.

The microstructure of several samples was characterized using both optical and scanning electron microscopy (SEM). The goal was to correlate features such as matrix penetration in between the opening of the fabrics, size and distribution of cracks, flaws, pores, and yarn damage, with mechanical properties. For the SEM observations fragments of specimens obtained after tensile tests were dried at 60°C and gold-coated.

2.4 Discussion of Test results

Effect of Fabric Type

Figure 2.4 below shows a combined load displacement graph of all the fabrics. A single layer of each fabric is tested in tension.

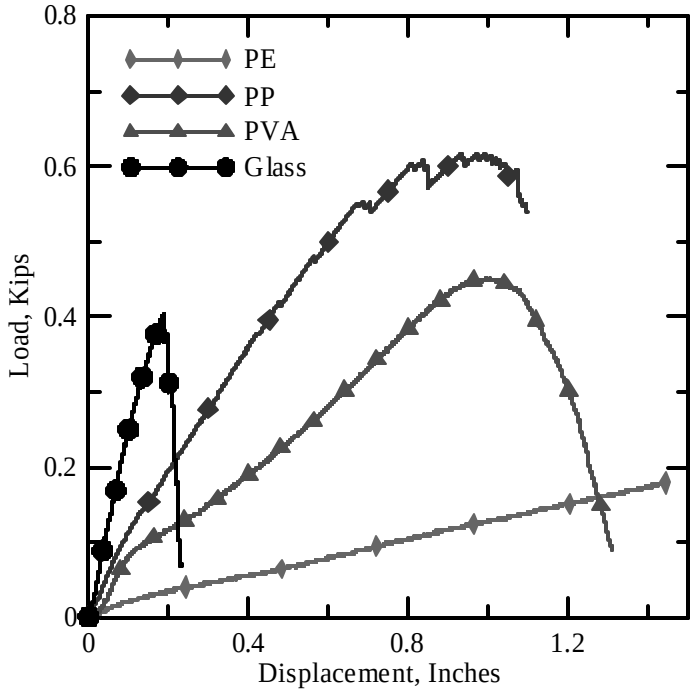

Fig. 2.4. Load Displacement plot for a single layer of fabric tested in tension

From the figure above, glass behaves in a brittle manner. The stiffness is very high for the fabric but the relative ductility is very low. Therefore the toughness of composites made of glass fabrics is low. On the other hand all the other three fabrics are very ductile. The best performance is given by polypropylene which has the highest strength and is also tough.

In figure 2.5 a combined stress strain plot of samples made up of eight layers of fabric is shown. The matrix properties are the same in all the samples. Again the behavior of glass composites shows a similar trend as that of the single layer of fabric. The stiffness is high which is indicated by the steep slope at the beginning and the brittle nature is depicted from the sudden failure that occurs in them. The samples with polyethylene have less strength, but are very ductile and they have lot of strain capacity.

Polypropylene and PVA have comparatively higher strengths than Glass and also have the advantage of being very ductile.

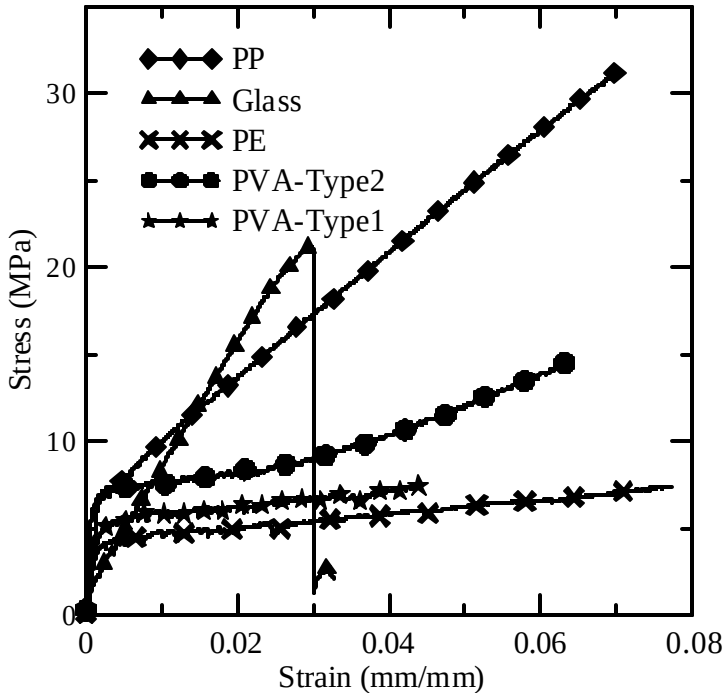

Fig. 2.5. Stress Strain plot of composites tested in tension

Figure 2.6a compares the effect of AR Glass and Polyethylene fabric types on the tensile stress strain response. In both cases similar matrix is used with super-plasticizer content of 0.2 by volume (Matrix #2, Table 2.1). Strain hardening behavior in the tensile response of both AR Glass and PE fabrics is observed even though the polyethylene fabrics are made from low modulus fibers. The tensile response of the glass composite shows a linear behavior up to about 3.5 MPa, beyond this level there is a knee in the curve and the stress measure increases with a reduced stiffness to levels as high as 20 MPa. The strain capacity of the sample is as much as 4%, and clearly shows the ability of the fabric to cause crack distribution. Similar to the glass fabric case, the curve of the PE fabric composite is linear up to about 4.5 MPa; beyond this level the formation of the

knee is quite evident as the post crack stiffness is significantly lower than the glass fabric case. The ultimate strength of the sample is in the range of 7 MPa at a strain level of about 4%. These general trends were obtained for all tested systems as shown in table 2.3 which presents the average tensile results.

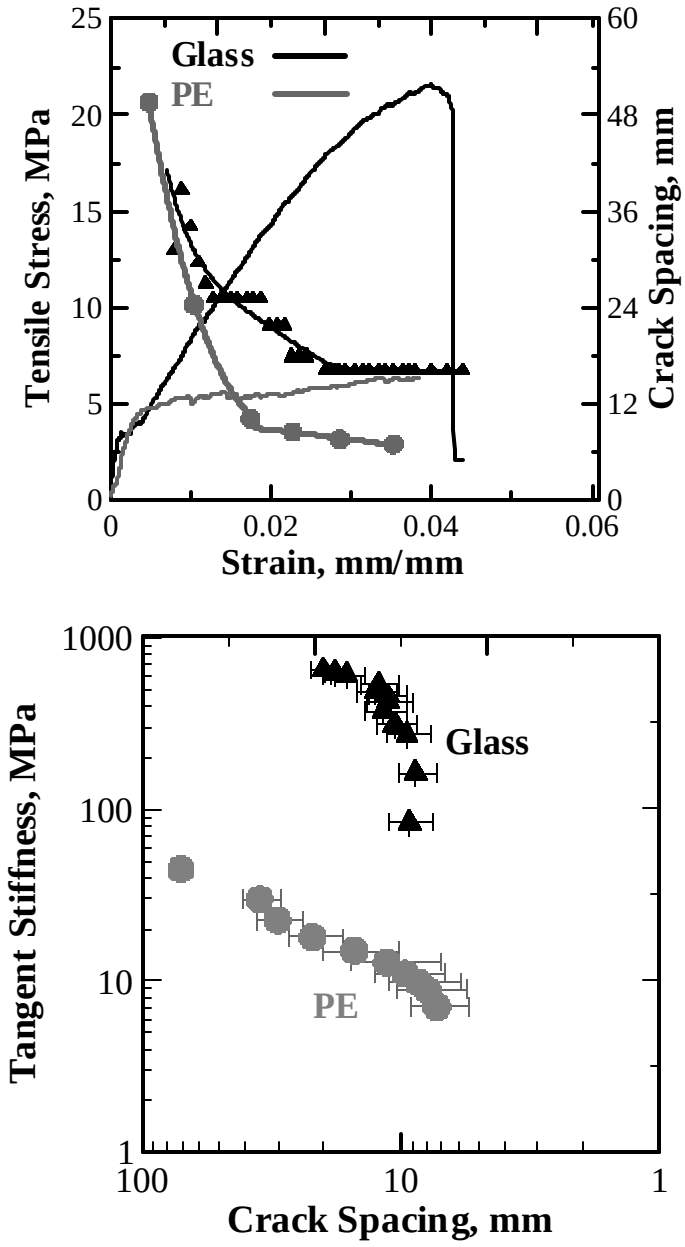

Fig. 2.6. Comparison of glass and PE fabrics composites: (a) tensile stress and crack spacing vs. strain, (b) tangent stiffness vs. crack spacing.

The crack spacing measurements are also shown in figure 2.6a for both glass and PE fabric composites. The figure shows a general decrease in the spacing during loading in both cases until a saturation level is reached as indicated by the curve becoming flat. Beyond this point, reduction in crack spacing is not observed, as further increase in the strain causes widening of existing cracks by fabric pullout. The PE composite shows much smaller crack spacing compared to the glass fabric composites. This indicates the greater ability of the PE fabrics in crack distribution, with ultimate crack spacing twice that of AR glass fabrics. The saturation crack spacing is about 18 mm for the glass composite and 8 mm for the PE composite. Such behavior can be related to the smaller size of the fabric opening in the PE system. Figure 2.6a clearly indicates that crack widening stage of the glass system starts at much later stage (80% final strain) than that of the PE system (50% final strain). This indicates that crack widening is the dominant mechanism in the PE system whereas in the glass system the composite stiffness is maintained over a longer range of response.

Comparative evaluation of both fabrics indicates that AR glass fabrics show a stiffer response in the post-crack stress-strain relationship than PE fabrics (figure 2.6b). The general trend of tangent stiffness and crack spacing decrease as a function of applied strain are shown in figure 2.6b where the correlation of crack spacing with the stiffness degradation is shown. It is clear that a major reduction in the values of the tangent stiffness takes place at very low strain values corresponding to matrix strength. This major reduction occurs at the point of initiation of cracks. Beyond this point, as the loading continues and successive cracks develop, there is a steady reduction in the composite stiffness. The stiffness degradation with AR glass samples is very high up to

the saturation crack spacing of 18 mm. This level correlates with the crack widening mechanism that take place at this stage of loading. While the stiffness reduction in glass is very high, it is seen that the tangent stiffness of PE at the post-cracked stage is quite lower as compared to glass as in figure 2.6b, but there is not a significant reduction in this value as a function of strain. Depending on the nature of data, this relationship can be represented in linear or logarithmic form. Empirical curve fitting parameters are presented in table 2.4. For the tangent stiffness comparison, composites with the best mechanical performance of each fabric system were chosen (glass fabric composite with addition of fly ash compares with PE fabric with plain matrix).

Based on the above discussion, one can differentiate three regions of response. The first portion of the curve represents the behavior of the un-cracked composite as a linear-elastic material, whereas the second portion, transverse crack formation and distribution in the matrix is the primary response. In the third region, crack widening is the dominant mechanism, mainly due to the properties of fabric and interface. Comparison of the mechanical behavior of the composites with the PE and AR glass fabrics shows that the primary mechanism of the PE composite is crack widening by fabric pullout and strengthening, whereas with the glass fabric composites crack widening is not the governing mechanism up to about 80% of its strength. The glass fabric is well bonded to the matrix and the tensile behavior is representative of the entire composite. Note that the volume fraction of the PE fabric is 9.5% and that of the glass fabric is only 4.4%.

Effect of Curing

Two curing processes were examined: accelerated curing 80°C in +90% RH, and 28 days curing at 23°C at 100% RH. The influences of the curing process on the mechanical response of glass fabrics composites are presented in Figure 2.7a. In general, the accelerated cured composites performed better than those cured for 28 days at room environment, suggesting that the 28 days specimens had not reached their maximum strength yet. The beneficial effects are observed mainly in strain capacity as presented in figure 2.7a. PE fabric composites showed a similar response. However, when high content of fly ash was added to the mix the trend was reversed and composite cured for 28 days at room environmental performed significantly better than the accelerated cured composite.

It may be expected that even with 7 days of elevated temperature curing, the flyash based composites are not fully hydrated. The brittleness observed at 28 days curing suggests improvement in the fabric-matrix interfacial properties, leading to improvement in bond strength. Such increased in bonding may cause fabrics to fracture prior to pullout. Crack widening is clearly seen in the large strain capacity of the composites with accelerated curing as shown in figure 2.7b. Comparison of the crack spacing profiles for both curing systems indicates that in composites cured for 7 days (accelerated), the crack spacing remains approximately constant throughout most of the strain range from 2.2% up to 5%, indicating that no new cracks are forming. Moreover, it is also observed that the stiffness in the post cracking stage of the 28 days cured specimens is greater than that of the accelerated cured specimen, further implying the improved fabric-matrix bond strength of the 28 days cured composite.

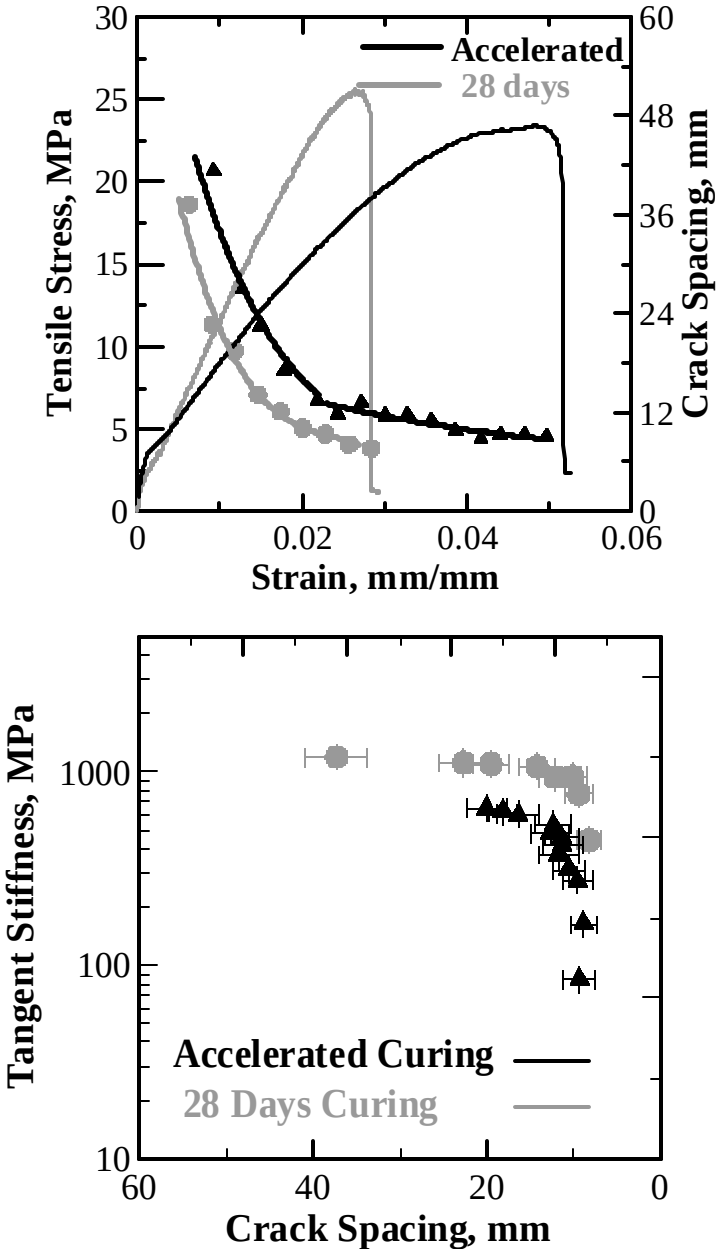

Fig.2.7. Effect of curing (a) tensile stress and crack spacing vs. strain, (b) tangent stiffness vs. crack spacing, of glass fabric composites with addition of fly ash

It may be expected that even with 7 days of elevated temperature curing, the flyash based composites are not fully hydrated. The brittleness observed at 28 days curing suggests improvement in the fabric-matrix interfacial properties, leading to improvement in bond strength. Such increased in bonding may cause fabrics to fracture prior to pullout. Crack widening is clearly seen in the large strain capacity of the composites with accelerated curing as shown in Figure 2.7b. Comparison of the crack spacing profiles for both curing systems indicates that in composites cured for 7 days (accelerated), the crack spacing remains approximately constant throughout most of the strain range from 2.2% up to 5%, indicating that no new cracks are forming. Moreover, it is also observed that the stiffness in the post cracking stage of the 28 days cured specimens is greater than that of the accelerated cured specimen, further implying the improved fabric-matrix bond strength of the 28 days cured composite.

Effects of pressure

After forming the laminates with the pultrusion process, pressure was applied to specimens to facilitate matrix penetration in between the fabric openings. In order to better understand the pressure effects, two levels were examined for glass fabric composites at 1.7 and 15.3 KPa (1:9 ratio).

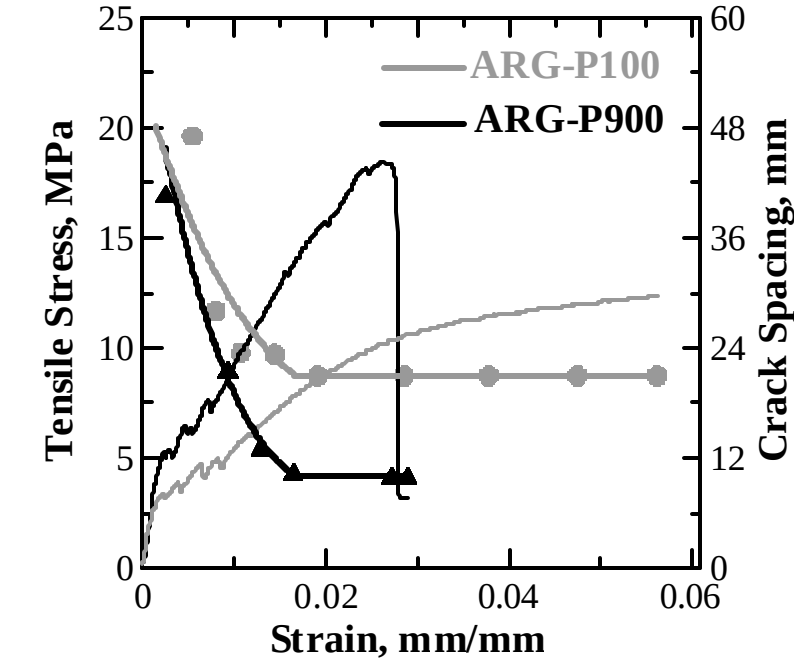

(a)

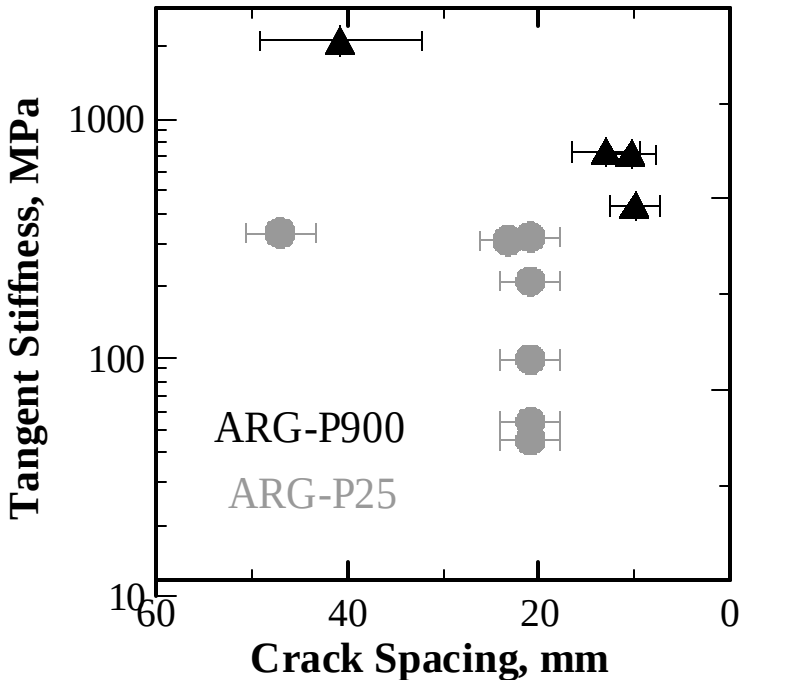

(b)

Fig. 2.8. Effect of the pressure apply after the pultrusion process: (a) tensile stress and crack spacing vs. strain, (b) tangent stiffness vs. crack spacing

Figure 2.8 presents the effect of the applied pressure on the stress strain and crack density-stiffness response. Many parameters such as initial cracking stress, post crack stiffness, ultimate strength, and also mean crack density are dependant on the level of applied pressure. By increasing the processing pressure the tensile strength is increased by about 40% (Table 2.3), however, the ductility is reduced as much as (40%). The tangent stiffness is also affected.

Table 2.3

Average tensile properties of the different pultruded specimens, exposed to accelerate curing

Specimen name	σ_{BOP} MPa	$\sigma_{ultimate}$ MPa	$\varepsilon_{ultimate}$ %	Toughness N/mm
ARG-P100	1.94	13.02	5.86	18874
ARG-P900	2.73	18.09	2.43	10319
ARG-SP0.2	2.52	21.06	3.11	13406
ARG-FA	1.68	22.68	5.56	25942
ARG-SF10	1.34	12.09	4.15	13909
PE-plain	1.7	7.21	3.73	4118
PE-SF5	2.39	7.56	5.62	10553
PE-SF10	1.55	5.49	2.69	4428

The composite with the high pressure is much stiffer throughout the loading cycle as in figure 2.8b. This may mainly be attributed to improvements at the fabric-matrix interface. The crack density increases as a function of applied hydrostatic pressure suggesting better

bonding and improved mechanical behavior for the composite with the increased pressure, while the composite with the low pressure developed fewer cracks suggesting a poorer bond in this case. Moreover, figure 2.8b also shows that crack widening is the operating mechanism of the low-pressure composites which do not show a significant cracking activity beyond a strain of 2%, a value less than half of the ultimate strain. In contrast, the entire tensile response in high pressure systems is controlled by multiple cracking mechanisms due to stress transfer between the fabric and the matrix. The above discussion suggests poor bond of the low-pressure system, and enhanced interaction between the fabric and the matrix for high pressure composites.

2.5 Microstructure

Evolution of damage was also observed under optical and scanning electron microscopes. The contribution of the reinforcing fabric to crack arresting and bridging is clearly observed in figure 2.9a. This figure shows a side view of glass fabric composite at the end of the tensile test. The crack propagates from one fabric layer to the next layer, through the thickness of the specimen. Such crack arresting and bridging mechanisms lead to high mechanical performance and energy absorption as shown by the tensile responses. It is also observed that the cracks develop both from one fabric layer to the next, in addition to delamination cracks between the fabric and the cement matrix.

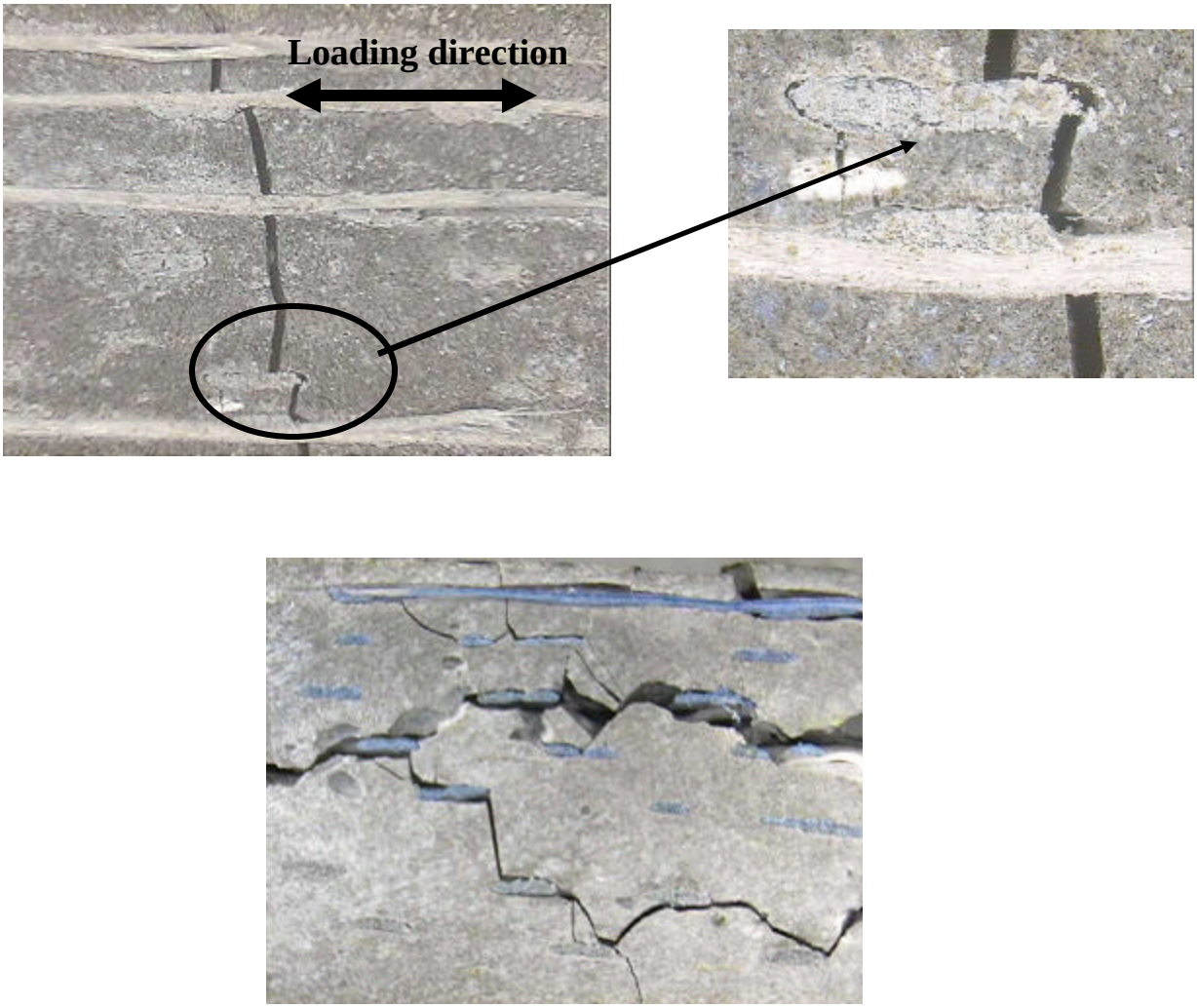

Fig. 2.9. Crack propagation in pultruded glass fabric composite: (a & b) crack propagation across the loading direction, (c) cracking across and along the loading direction at failure.

Crack arresting and bridging by fabric layers is observed for the PE fabric system in figure 2.10. The yarns in this woven fabric have a wavy geometry and the matrix cracks near the junction of the fabric near the perpendicular yarns. When the standing wave of the reinforcing yarn is straightened during tensile loading, local stresses are

developed in the matrix around the pressed perpendicular yarn, leading to damage and cracking at this area, as clearly observed in figure 2.10.

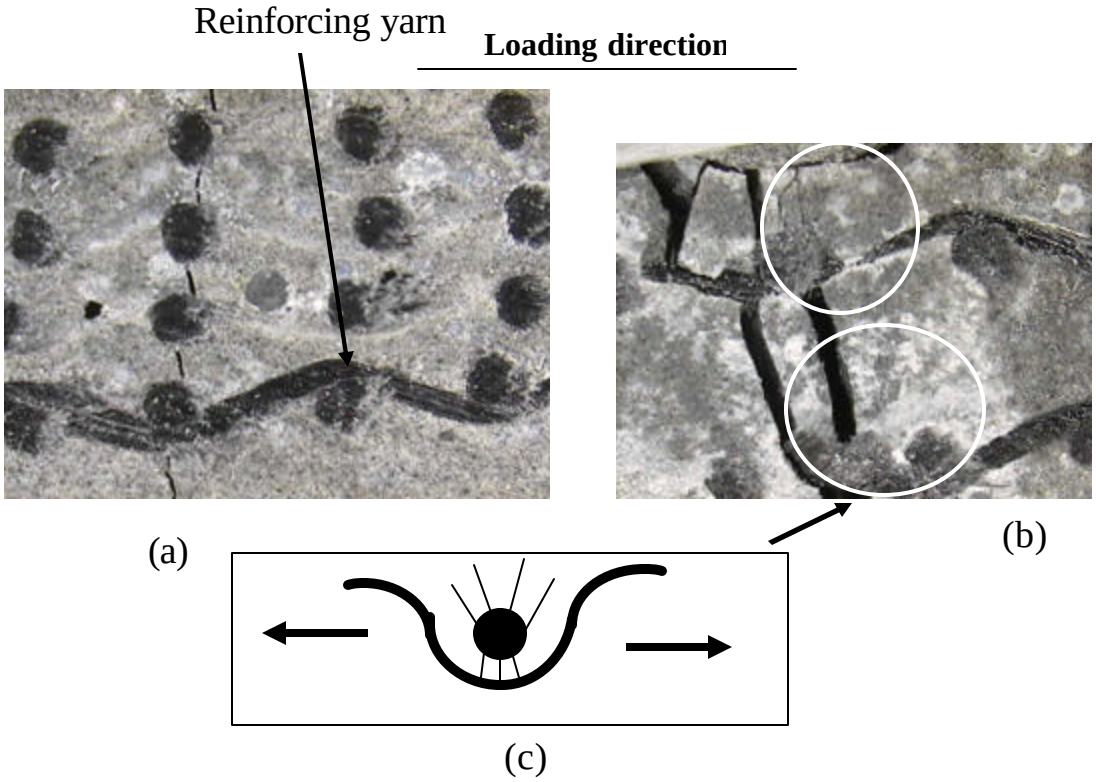

Fig.2.10. (a & b) Crack propagation across the loading direction of woven PE fabric cement composite and (c) schematic description of the stresses developed at the fabric junction

The failure of the fabric at the end of test is obvious in figure 2.11a which shows the fracture area of the glass fabric composite. Not such failure was observed with the PE fabric composite, since testing was terminated before any damage occurred in the fabric. The low mechanical performance of the composite with the high content silica fume

(ARG-SF10, PE-SF10, Table 2.3) might be explained based on the observations presented in figure 2.11.

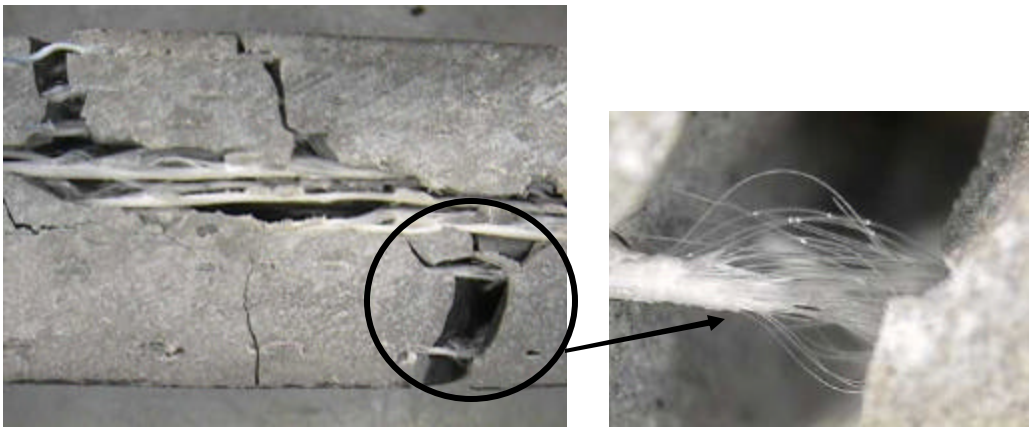

Fig. 2.11. Failure of the fabric at the end of testing in glass-fabric composite

It is clear that during manufacturing, the high viscosity of the high content silica fume mix (shear stresses of 6972 D/cm^2) caused some damage to the yarn surface of the fabric in both fabric systems, glass in figure 2.12a and PE in figure 2.12b. Such damage was observed mainly at the surface of the yarn located along the pultrusion process. The epoxy coating was peeled-off the surface of the glass yarn as it passed through the matrix bath during the pultrusion process, whereas with the PE fabric system damage is observed at the junction of the fabric. Such damage was not observed for the mix with lower content of silica fume or for the yarns perpendicular to the pultrusion process as Figure 2.13 c.

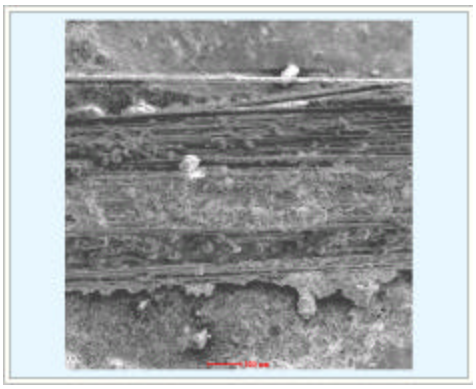

(a)

(b)

(c)

Fig. 2.12. SEM micrographs of the fabric in pultruded cement composite with high content of silica fume (10%): (a) glass yarn along the pultruded direction, (b) PE fabric at the junction of the yarns, (c) glass yarn perpandicular to the pultrusion direction

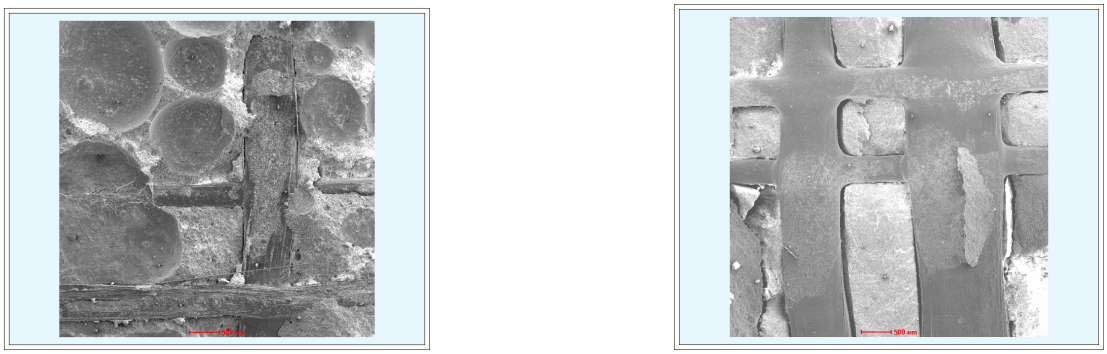

(a) (b)

Fig. 2.13. SEM micrographs of fabric embeded in cement composite with different content of superplastisizer: (a) high content (matrix #3 in Table 2.1) and (b) with low content (matrix #1 Table 2.1).

CHAPTER 3

FLYASH BASED COMPOSITES

The penetration of cement paste in between the opening of the fabrics is a controlling factor in the ability of the system to develop and maintain the bond. Such penetration is dependant on the size of the fabric opening and the viscosity (rheology) of the matrix. Also, the viscosity of the fresh mix is an important factor in the pultrusion process, if the mixture is too stiff the fabric may be damaged as it goes through the cement bath, however, if the mixture is too soft, not enough matrix will adhere to the fabric as leaves the cement bath. The use of additives such as fly ash can influence the viscosity of the fresh cement mixture.

This chapter examines the effects of using flyash as an integral part of the matrix system at levels of up to 80% cement replacement. Bonded glass mesh fabrics were used to produce the pultruded composites. Effect of the processing parameters on the mechanical properties, fabric-matrix bond, and micro structural characteristics of cement composites are studied using tensile tests. A micro structural analysis was also conducted and correlated with the mechanical performance of the composite and interface bond.

3.1. Experimental

Materials

The AR glass fibers were with tensile strength of 1270-2450 MPa, elastic modulus of 78,000 MPa, filament diameter of 13.5 microns with 400 filament per bundle.

The fibers were used in a fabric with 2 yarns per cm in each direction (warp and weft). The straight warp and weft yarns were glued together at the junction points. The glass fabric is shown in figure 3.1.

Four different matrix formulations consisting of three percentages of class F flyash along with a control sample were used. The fly ash was used as replacement of the cement. The mix designs used are presented in table 3.1. In all cases 5% of silica fume was used and the water/binder ratio by weight was 0.375. With addition of flyash the workability of the mix increased which may be attributed to the fineness of the pozzolanic material. Rheology experiments were conducted to document the change in workability of the mix.

Table 3.1

The Mix Design (by volume) used in the study

Mix ID	Mix Design	Cement Content	Fly ash Content	Silica Fume	W/C Ratio
A	Control	95%	0	5%	0.375
B	40% FA	55%	40%	5%	0.375
C	60% FA	35%	60%	5%	0.375
D	80% FA	15%	80%	5%	0.375

:

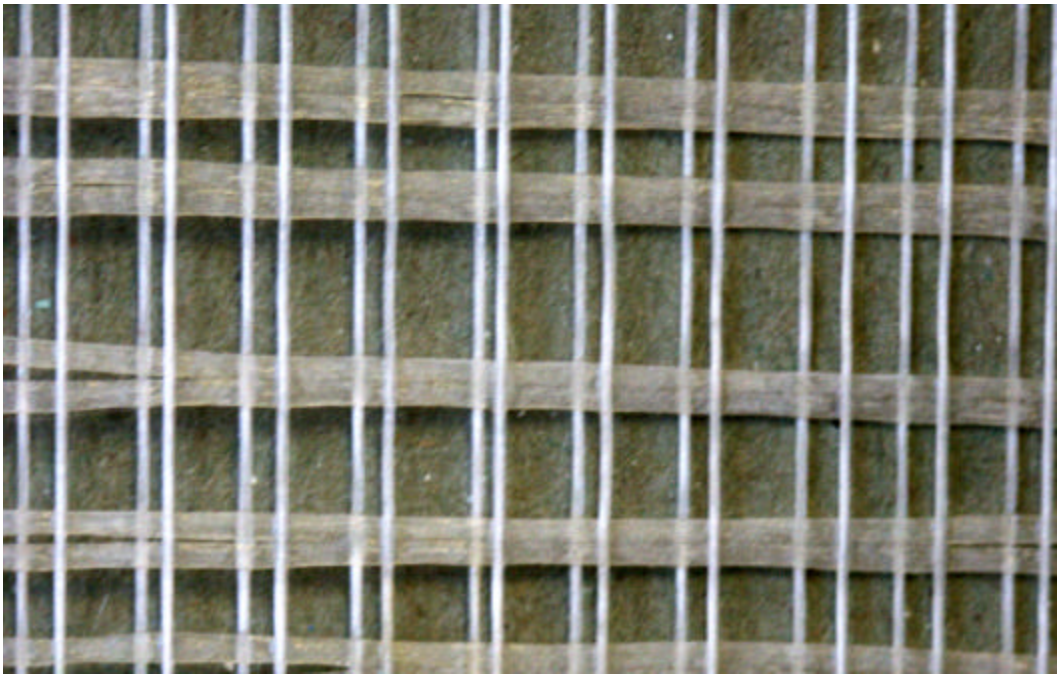

Fig. 3.1. The bonded AR Glass Fabric Mesh.

3.2 Testing

Mechanical performance

Closed loop control direct tensile tests were performed on all the specimens using a MTS testing machine with a capacity of 89KN. Metal plates with dimension of 25x30 mm were glued on the surface of the specimen at the grips to minimize damage. The tensile load and elongation were recorded and converted to stress-strain response. The tensile strength, stiffness, ductility, strain capacity, and cracking parameters were measured. A procedure was developed to quantitatively measure the crack spacing parameters. Photographs were taken of the samples at fixed time intervals to measure the crack formation. A monochromatic light source was used to illuminate the specimen under test while a digital frame grabber captured images at 15 second intervals under an

increasing displacement. Using digital processing toolbox of MATLAB, the images were processed to quantitatively measure the crack spacing and density as a function of the applied strain. Details of this procedure are mentioned in chapter 4 which primarily deals with the crack spacing measurements.

Microstructure

The microstructure of several samples was characterized using both optical and scanning electron microscopy (SEM). The goal was to correlate features such as matrix penetration in between the opening of the fabrics with the flyash content. For the SEM observations fragments of specimens obtained after tensile tests were dried at 60°C and gold-coated.

3.3 Discussion of Test results

Effect of Flyash

Use of flyash and silica fume in matrix are beneficial since the pozzolannic reactions densify the matrix, reduce the available Calcium Hydroxide at the interface transition zone, and improve the long-term durability of composites with low durability fabrics. Moreover, the particle morphology of the flyash can improve the rheology of the matrix. The penetration of cement paste in between the opening of the fabrics is a controlling factor in the ability of the system to develop and maintain the bond. Such penetration is dependant on the size of the fabric opening and the viscosity (rheology) of the fresh matrix. Figure 3.2 shows the performance of five replicate samples with the mix containing 60 % flyash. In this case, a tensile strength of about 25 MPa at a strain

capacity of about 5% are observed. The initial response of the composites is linear up to the Bend Over Point (BOP) achieved at around 5 MPa. The BOP level begins with the formation of an isolated crack and ends when it has propagated across the entire width of the specimen. The fibers delay the localization by transferring stresses back into the matrix. Even when a full crack occurs across the cross section, the fibers are able to transfer the total load across to the other side. Uniform placement of glass fibers within the matrix activates them as soon as cracking takes place and the load increases over a large strain range up to about 3 %. It is also noted that after the BOP, the stiffness of the composite decreases, but the load carrying capacity remains relatively uniform over a large strain range. It is during this region that significant microcracks form throughout the matrix material. The ultimate tensile strength and strain capacity are in the range of 25 MPa at 2.8% strain. Compared to other fiber reinforced composites such as GFRC, these materials are as much as five times stronger, and six times more ductile, while compared to plain cement based materials, these proportions are eight and four hundred times.

The samples presented in figure 3.2 were all tested after 7 days of curing. With the addition of pozzolanic materials, the rate of gain in strength is reduced; hence additional curing time may improve the properties. As expected, there is a drastic improvement in the performance after 28 days of curing. A comparison graph of the mix with 40 % flyash content at 7 and 28 days curing cycles is shown in figure 3.3. The samples gain both strength and post crack stiffness with curing, but lose the ductility as the bond between the matrix and the fabric is improved with curing.

A comparison of all the representative samples of various percentages of flyash along with a control sample (0% flyash, 5% silica fume) is shown in figure 3.4a. The optimum level of improvement in the mechanical performance is observed in cement composites with 60% flyash replacement of cement. Note that at the 7 day stage, the variation in the data is mostly observed in the post BOP level. The 80 % flyash mixes show similar behavior as the control sample with stiffness and strength lower than that of the 60 % mixture. The 40 % flyash has the lower post crack stiffness. The mechanical performance results are better represented when we evaluate the 28 days results as shown in figure 3.4b. All the samples show a significantly higher strength than the plain paste mixtures. Comparing the three flyash levels, the optimal flyash content can be predicted between 40 and 60 %. This may be attributed to the better durability of AR glass mesh in the presence of a high flyash matrix. All the results are presented in table 3.2.

Table 3.2

Average Mechanical Properties of samples from each group (7 and 28 day curing period) along with the standard deviation values

Mix ID		Days	Ultimate Strength (MPa)	Ultimate Strain (mm/mm)	Initial Stiffness (MPa)	Toughness (MPa)
A	Average	7	19.40	0.030	3520.7	0.367
	(Std. Dev)		(3.74)	(0.003)	(177.5)	(0.072)
	Average	28	21.45	0.0254	4981.2	0.358
	(Std. Dev)		(2.39)	(0.002)	(211.1)	(0.053)
B	Average	7	18.73	0.080	1651.3	1.062
	(Std. Dev)		(3.04)	(0.030)	(112.1)	(0.315)
	Average	28	23.79	0.0258	4753.2	0.394
	(Std. Dev)		(2.49)	(0.003)	(151.3)	(0.074)
C	Average	7	24.27	0.024	2360.4	0.384
	(Std. Dev)		(2.09)	(0.003)	(125.1)	(0.069)
	Average	28	28.69	0.0255	5015.2	0.482
	(Std. Dev)		(3.71)	(0.001)	(178.2)	(0.075)
D	Average	7	19.09	0.0283	2575.3	0.417
	(Std. Dev)		(7.35)	(0.0108)	(201.3)	(0.206)
	Average	28	23.45	0.0170	4051.1	0.288
	(Std. Dev)		(3.94)	(0.003)	(215.5)	(0.107)

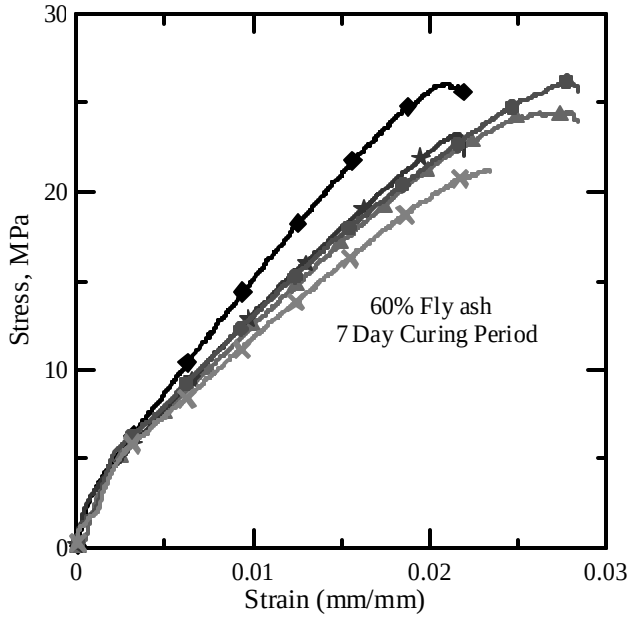

Fig. 3.2. Tensile Stress Strain plot of samples with 60% fly ash content.

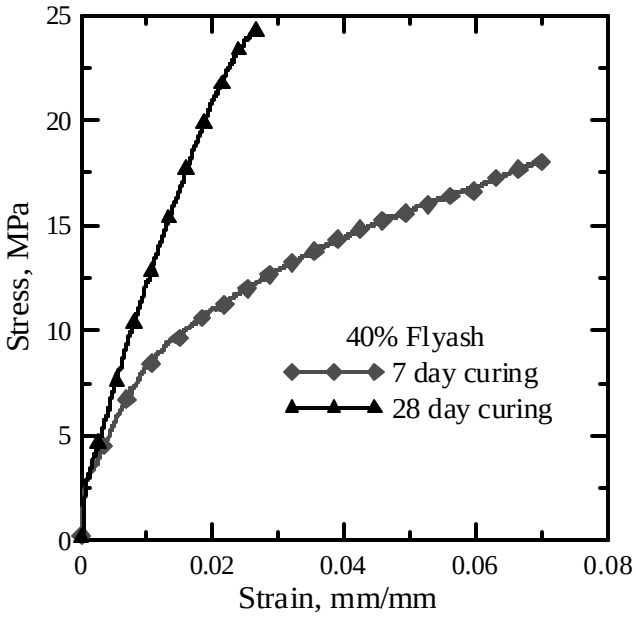

Fig. 3.3. Comparison of the tensile stress strain response of samples with 40% Fly ash content at 7 and 28 days.

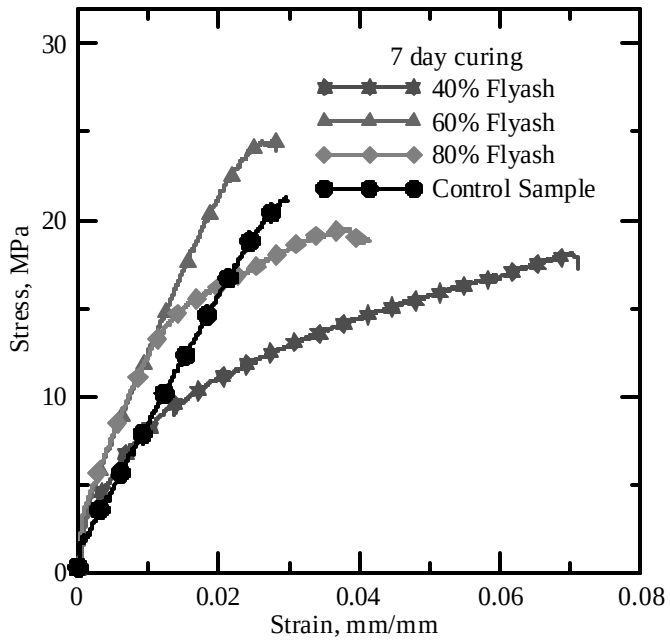

(a)

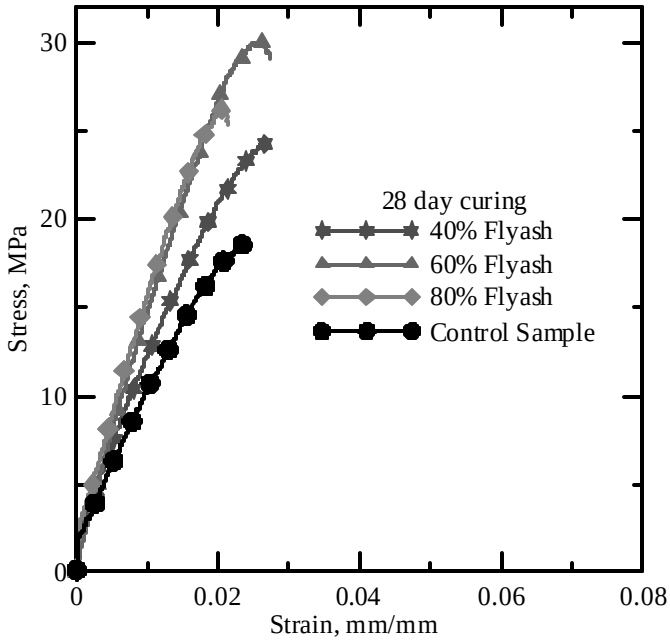

(b)

Fig. 3.4. Comparison of stress strain response of specimens with different fly ash contents and control sample (a) after 7 days (b) after 28 days

Crack spacing measurements conducted on the 7 and 28 day samples are shown in figure 3.5. In general when comparing the different composites, lower crack spacing suggests higher interfacial bond strength for systems having similar fabric content. Such difference in crack spacing is clearly observed suggesting relatively low bond strength at 7 days curing. Once the initial cracking has taken place, the cracks widen in the case of 7 day samples. On the contrary in 28 day samples, since the bond is so strong, crack formation takes place till the point of failure as determined by as mush as half the crack spacing of the 7 day cured samples. (10 mm for 28 day cured samples as compared to 20 mm for 7 day cured samples).

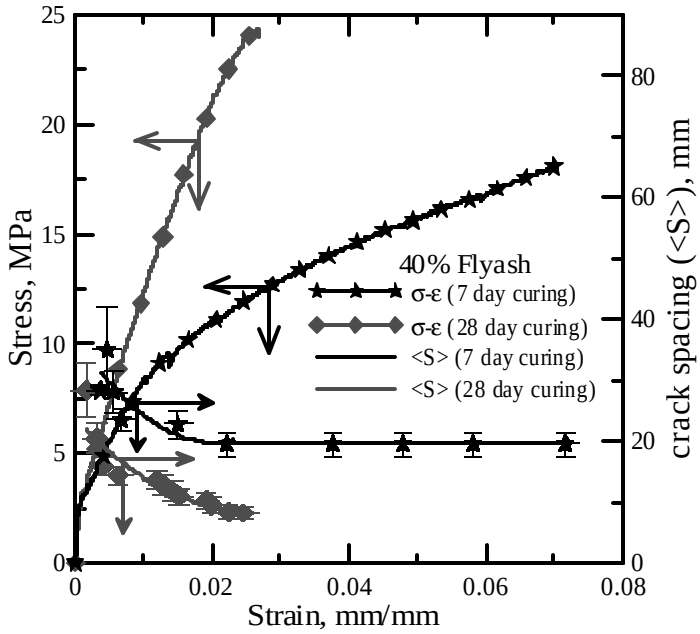

Fig 3.5. Showing the Crack Spacing Characteristics along with the Stress strain of samples at 7 and 28 days.

Effect of Accelerated Ageing

Accelerated ageing was conducted by storing specimens in a saturated calcium hydroxide solution for 28 days. The temperature inside this chamber was maintained at 80ºC. The influences of the curing process on the mechanical response of glass fabrics composites are presented in figure 3.6. It can be seen with reference to two different levels of flyash that there is no significant difference in the mechanical performance at the two different levels.

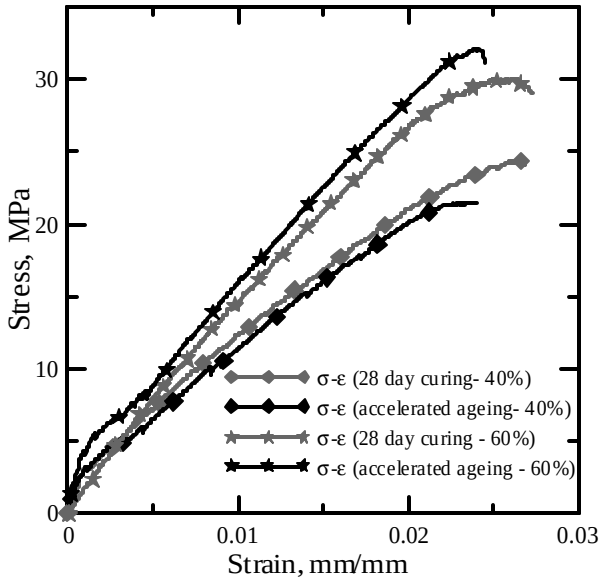

Fig. 3.6. Stress strain response after 28 days accelerated ageing compared with control samples.

3.4 Rheology

The difference in the mechanical behavior of the samples at different curing periods due to the presence of flyash could also be attributed to the rheology of the matrix. Tests were conducted on the mixes using a Brookefield Rheometer. The shear rate was varied during the tests ranging from a higher rpm value (20) at the start to a lower value (10). Figure 3.7 is a plot of the shear strength versus the shear rate. The results in the plot indicate that the viscosity of the control samples increases much faster as compared to the three different levels of flyash indicating that the presence of flyash causes a slower rate of stiffness gain. The yield strength of the sample decreases with the addition of flyash also. This may explain the ability of the composites with high flyash content to develop a better bond strength with the fabric due to the ability of the fresh pasted to infiltrate the fabric openings Again with time the shear rate increases but with the increase in the amount of flyash, this strength gain is very slow.

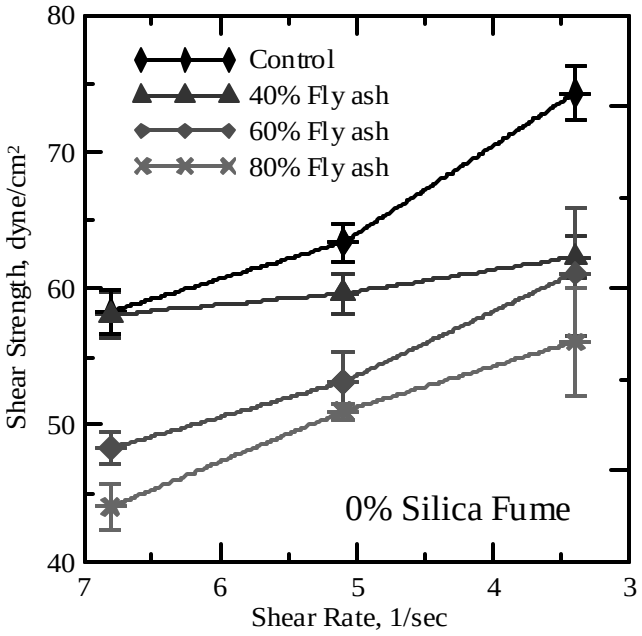

Fig. 3.7. Shear strength vs. shear rate plots for various levels of flyash

Table 3.3 below shows the various yield strength levels along with the viscosity, for all the different mixes that were in consideration. The yield stress values indicate the slow strength gains of the flyash samples. There is drastic difference between the values at 40% flyash level and 60% level. The table yet again emphasizes the lower strength of flyash based composites at 7 days as compared to 28 days.

Table 3.3

Yield Strength and Viscosity values for the four mix designs

Mix	Yield Stress ($dyne/cm^2$)	Viscosity (centipoises)
Control	48.24	2.98
40% FA	45.72	1.76
60% FA	38.66	2.84
80% FA	30.02	4.02

Similar studies were carried out with mix with different Silica Fume contents along with fly ash to see the combined effects. Figure 3.8 below shows a set of samples with a silica fume content of 5 % and figure 3.9 shows samples with silica fume content of 10%. The addition of silica fume increases the fluidity of the mixes further and the setting time is increased.

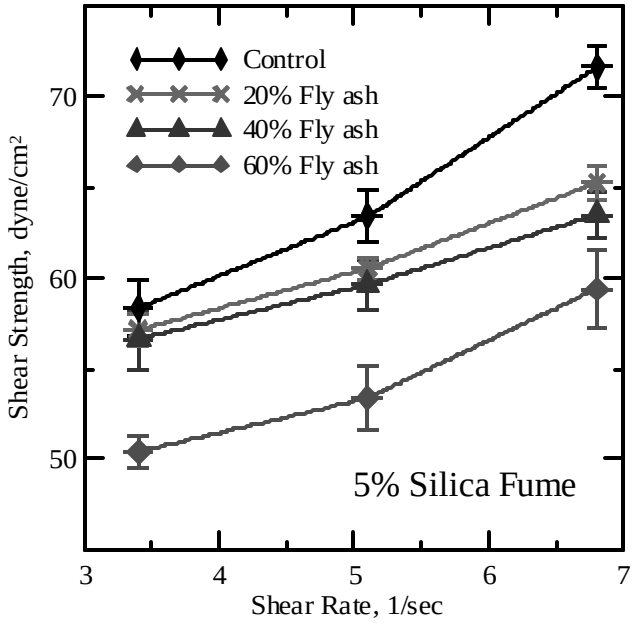

Fig. 3.8. Shear strength vs. shear rate plots for various levels of flyash with 5% SF

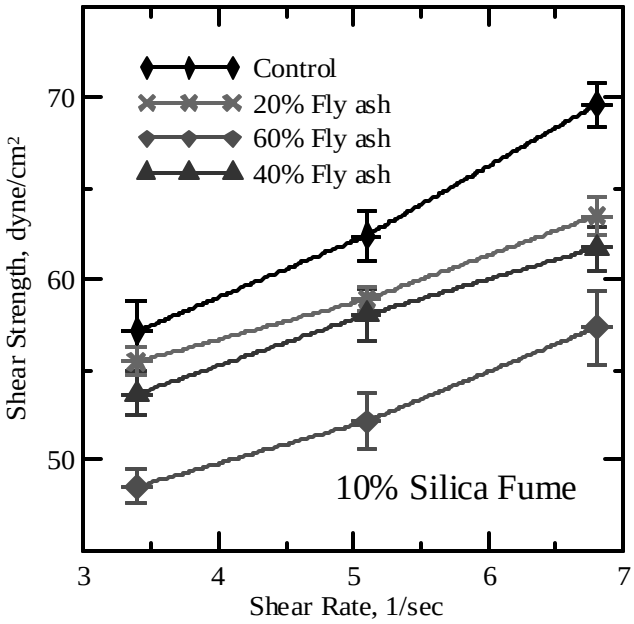

Fig. 3.9. Shear strength vs. shear rate plots for various levels of flyash with 10% SF

Thus the effect of Silica fume is to increase the workability. The reason behind this is that silica fume has very fine particles as compared to cement, and therefore the voids between the cement particles is filled by silica fume. This causes the mix to be more fluid but it retards the strength gain of the mix.

3.5 Microstructure

The microstructure of the specimens was studied so as to understand the impregnations aspects of the samples with flyash. The specimens were observed under scanning electron microscope. The goal of this part of the study was to see how the flyash addition improves the microstructure of the fabric paste bond. In figure 3.10a, it is seen how the flyash occupy the capillary voids and the transition zone in the vicinity of the inter yarn spacing. This may explain why the bonding is so strong in mixtures with high levels of flyash. The flyash particles result in a lower viscosity and better flow of the matrix so around the surface of the fabric. This is clearly reflected from figure 3.10b.

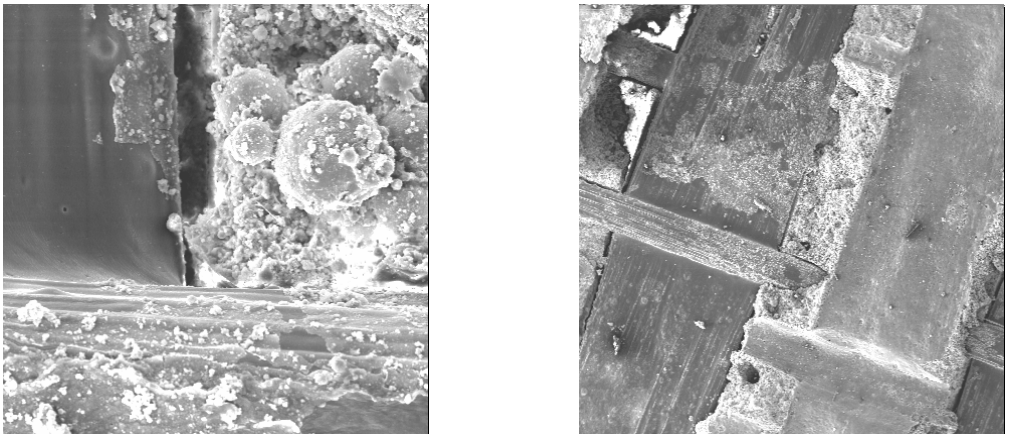

(a) (b)

Fig. 3.10. a) Fly ash (60% mixture) in the vicinity of the yarn junction b) The matrix penetration in between the two adjacent fabric layers (60% mixture).

CHAPTER 4

CRACK SPACING MEASUREMENT AND STIFFNESS DEGRADATION

The behavior of fabric-cement composites exposed to tensile loads is characterized by multiple cracking. These distributed transverse cracks form gradually as the composite is loaded beyond the initial cracking stages. The nature of multiple cracking and the resulting stress-strain curve, toughness, and strength, are dependent on the properties of the reinforcing fabrics, the cement matrix, as well as the interface bond developed. Therefore, parameters which lead to crack formation ultimately control the fabric-cement composite properties. Microstructural features such as crack spacing, width, and density allow formulation of the damage evolution as a function of macroscopically applied strain. This can help in correlating various fabric types and mixture formulations with increases in modulus of rupture, ductility, and increased strain capacity of different composites. The composite stiffness in the post crack range is an important property that should be considered. A general relationship between the crack spacing and the stiffness at various stages of loading can be compared with the damage development as the strain increases.

The objective of this study was to develop tools to formulate the damage evolution of fabric-cement composites as a function of the applied strain under tensile loading. This was developed by analyzing the changes in crack spacing under loading and correlation of crack pattern, crack spacing, and stiffness degradation at different strain levels of various composites. Photographs of crack development were taken throughout

the loading of the composite. The crack spacing for a particular stage of loading was computed using image-processing techniques. The change in composite stiffness during loading was also monitored. A general profile correlating between the crack spacing and the stiffness at various stages of loading was predicted. Finally, the microstructure of the different composites was characterized and correlated with their mechanical properties using optical and scanning electron microscopy. The test procedure is the same as discussed earlier. This chapter will deal with the crack spacing analysis of the photographs taken during the tests. A correlation between the strain applied and the crack development will also be discussed. This is then used in the theoretical modeling which is discussed in the next chapter.

4.1 Crack Spacing Measurements

By taking photographs of the specimen at regular time intervals, the crack development throughout the loading cycle of the tensile tests is recorded. A monochromatic light source was used to illuminate the specimen while a digital frame grabber captured images at 15 second intervals. Figures 4.1a and 4.1b present the crack development at early stage (recorded at $\varepsilon = 2.72\%$) and late stage (recorded at $\varepsilon = 4\%$) respectively.

Using digital processing toolbox of MATLAB, the images were processed to quantitatively measure the crack spacing and density as a function of the applied strain using a two step approach. During the first step, newly formed cracks of each image were traced and added to data from previous loading increment. Figure 4.1c represents

the profile of the trace of cracks for Figure 4.1b. The second step measured the crack spacing from the traced cracks as shown in Figure 4.1d.

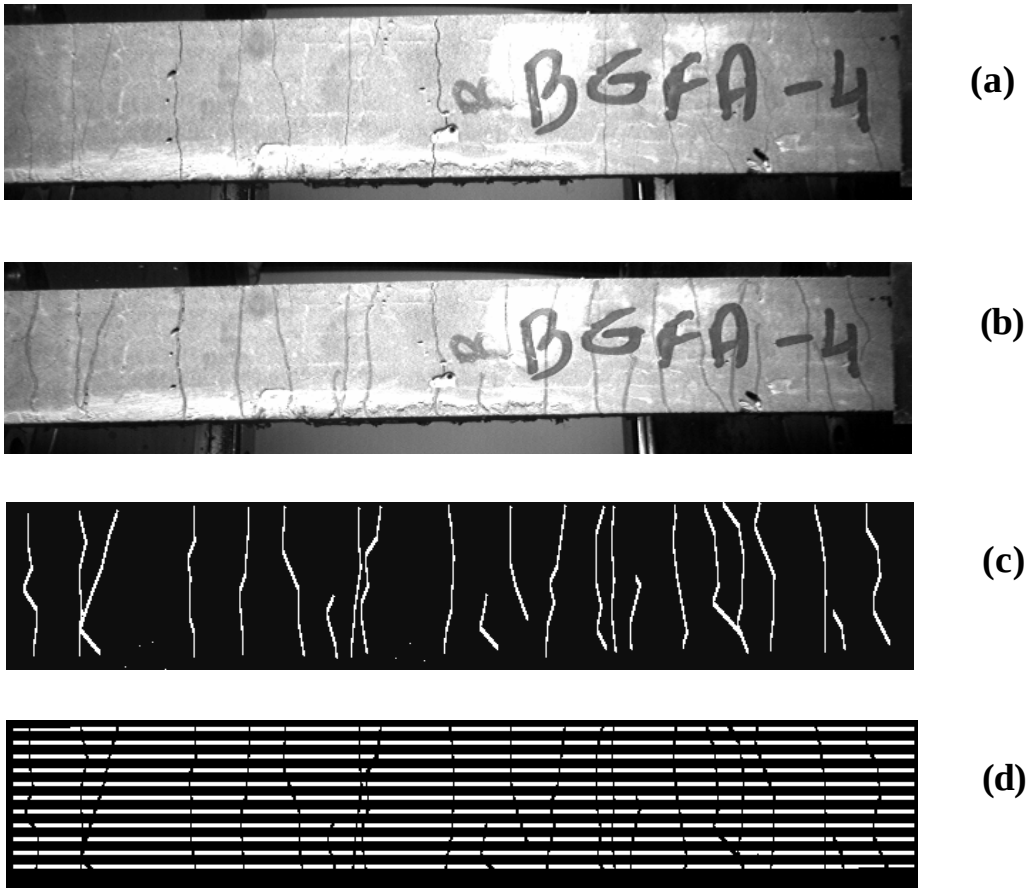

Fig. 4.1. Image analysis procedure: (a) & (b) images of specimens during tensile tests, (c) trace lines of cracks, (d) vertical lines for distribution of crack spacing

The procedure for measuring the crack spacing was as follows: An image consisting of a series of parallel lines was generated. By conducting a binary "AND" operation the points of intersection of parallel lines with the cracks were identified. A second binary operation of "OR" between the intersection points and the parallel spacing lines, broke up the straight lines into segments representing a crack spacing measurement. This is shown in Figure 4.1d. The next step was to count the distribution of the length

segments and statistical parameters of crack spacing. The crack spacing was measured in pixels, and the image was calibrated using conventional techniques to convert the size of a pixel to length measures. This procedure was published by Stang, Mobasher, and Shah. (1990)

The crack spacing obtained from the program is in terms of pixels. This needs to be converted in to standard units (inches or mm.). This can be done using a calibration technique in which one can take horizontal and vertical photographs of anything of known length (in our case a ruler). Figure 4.2 below shows a photograph taken for calibration purposes. One can trace an exact known length along this using the pixval command of MATLAB. With the help of a small sub routine we can find out the calibration that needs to be done to convert the pixel values into known units. Table 4.1 summarizes the same which has the standard readings taken by the subroutine for a given length.

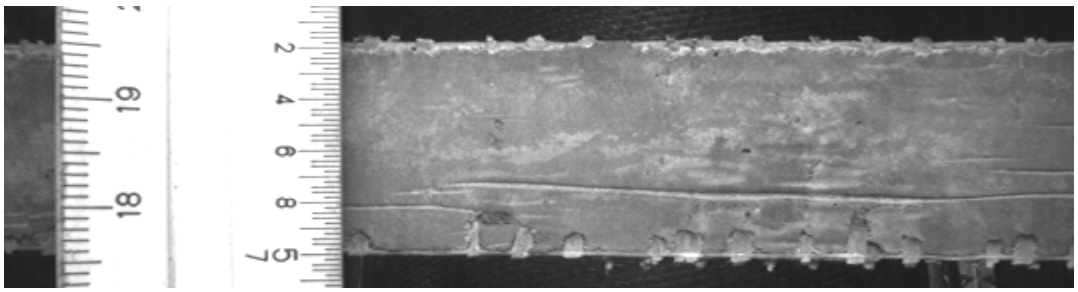

Fig. 4.2. Photograph used for calibration

Table 4.1

Calibration readings

Figure No.	Type of Scale	Reading			Average
		1	2	3	
1	Vertical	151	150	151	150.67
2	Vertical	152	152	152	152.00
3	Vertical	149	151	151	150.33
4	Inclined	132	133	133	132.67
5	Inclined	131	131	132	131.33
6	Horizontal	132	133	133	132.67

A typical crack spacing curve is shown in figure 4.3 below. The curve is defined by four parameters as shown in the figure. These four parameters are studied for al l the different mix designs and fabrics to get a general trend. This will take us a step further into our theoretical model and these parameters will play an important role for modeling purposes. All the four parameters depend on the properties of the matrix and fabric type. The parameter S_1 defines the crack widening phase. This is the constant crack spacing that indicates the change from the crack development to the crack widening stage where the further crack formation stops. The parameter ε_{mu} defines the initial cracking phase. It gives the point at which the cracking takes place and the stiffness degradation begins. S_0

and α are the parameters that dictate the slope in the crack development zone. The study in this chapter is basically involving these parameters and different matrix and crack formation.

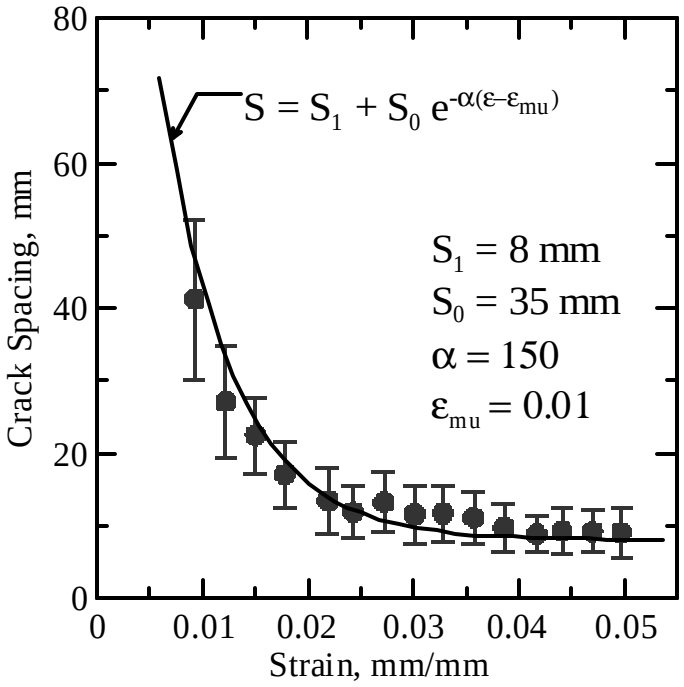

Fig. 4.3. Typical Crack Spacing Curve for a sample with AR Glass and 40% flyash

Table 4.2 below gives the representative values of the samples with different mix designs and fabric types. These Empirical curve fitting parameters are used in the theoretical model. From the nature of the data the relationship was worked to be a typically exponential and of the form as given in the table.

Table 4.2

Crack Spacing parameters with respect to strain

Specimen name	Crack Spacing Equation ($S = S_1 + S_0 * EXP(-\alpha * Strain + \varepsilon_{mu})$)			
	S_1 (mm.)	S_0 (mm.)	α	ε_1
ARG-P900	9	10	140	0.011
ARG-P100	18	22	50	0.008
ARG-SP0.2	15	10	180	0.010
BGFA-4	8	35	150	0.010
ARG-SF10	22	10	180	0.007
Average	14.4	17.4	140	0.0092
Std. Dev	5.94	11.12	53.39	0.0016
PE-plain	7	20	170	0.010
PE-SF5%	10	13	190	0.005
Average	8.5	16.5	180	0.0075
Std. Dev.	2.12	4.95	14.14	0.0035

4.2 Measurement of Stiffness degradation from the Stress-strain plots

As cracks get induced in the sample the stiffness goes on reducing. The effect can be seen from the way the stress-strain curve deviates from linearity. We all know that the stiffness is the slope of the stress-strain curve. In order to measure the stiffness between two points one can use software's like SIGNO that can directly measure the slope between two points. On the other hand, we can also calculate the slope of the line joining two points using geometric formulae. Both the methods give same results. The stiffness generally shows a decreasing trend as we go to higher strains. Plots that show the way the stiffness degradation has taken place as we go to higher strains and also the degradation of stiffness with respect to the crack spacing helps us understand the behavior of the fiber reinforced concrete. These plots are shown in the results and discussion section. The general trend of these plots is such that the initial stiffness reduction is very fast. This is the stage when concrete cracks till the point when the contribution of concrete reduces. After the initial steep degradation the curve becomes more or less constant indicating the stage when the concrete has completely cracked. Atypical stiffness degradation curve along with the crack spacing versus strain plot is shown in figure 4.4 below.

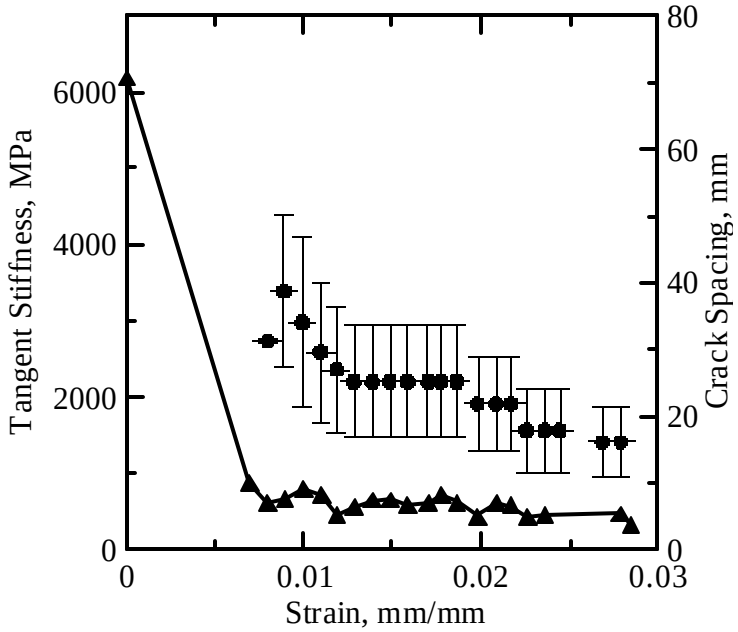

Fig. 4.4. Typical Stiffness degradation plot along with the crack spacing evaluation for a sample with AR glass and no super-plasticizer

Table 4.3 below gives the tangent stiffness degradation constants for the various mix designs. For the tangent stiffness comparison, composites with the best mechanical performance of each fabric system were chosen (glass fabric composite with addition of fly ash compares with PE fabric with plain matrix).

Table 4.3

Stiffness degradation constants for different specimen types

Specimen name	Stiffness Equation (Z = M*EXP (-L*Strain)	
	M	L
ARG-P900	1357.23	87.65
ARG-P100	1260.15	98.43
ARG-SP0.2	1596.77	56.97
BGFA-4	1575.75	57.78
ARG-SF10	1275.13	54.57
Average	1413.01	71.08
Std. Dev	162.59	20.44
PE-plain	80.50	82.85
PE-SF5%	100.29	105.84
Average	90.39	94.35
Std. Dev.	13.99	16.26

CHAPTER 5

THEORETICAL MODEL

A theoretical model is presented here to relate the properties of the matrix, fabric, and interface and the damage parameters such as the crack spacing parameters to the overall mechanical response of composites. Results are used to explain the effects of various materials and processing parameters on the mechanical response of cement based fabric reinforced composites. Variables studied include simulation of the effects of fabric types, strength increase, ductility increase, and increased strain capacity. The load deformation results obtained through experiments are simulated using a model which relates the crack spacing evolution and stiffness degradation to the applied strain. Model simulation data is compared with the wide range of experimental tests to verify the model.

5.1 Nonlinear Stress Strain Response

A comprehensive experimental program was conducted to study the effect of fabric type, matrix formulations, and also the processing parameters. The results of this study are presented in an earlier publication by Peled and Mobasher (2004). Portions of the experimental program are used in this manuscript to address the modeling challenges for these systems.

Figure 5.1 represents a typical tensile stress strain response of AR Glass fabric reinforced cement composite. The tensile response shows a linear behavior up to about

3.5 MPa, beyond this level the stress-strain response becomes nonlinear, and the major change in the stiffness of the sample occurs at around 4-5 MPa at a point defined as BOP. The BOP is characterized by a knee in the curve. Beyond the BOP, the stress increases showing strain hardening behavior up to a stress level of about 17 MPa. Strength of this class of composites can reach as high as 20 MPa with an ultimate strain capacity of 4%, clearly showing the ability of the fabric to cause crack distribution.

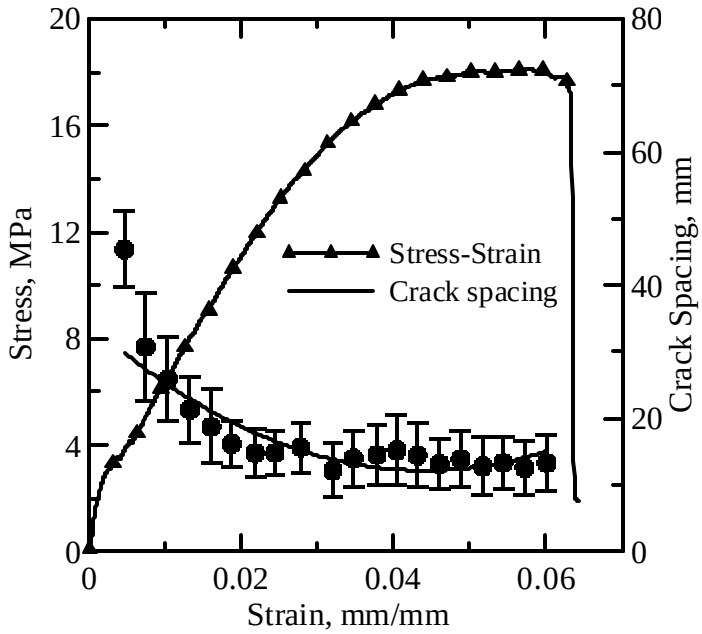

Fig. 5.1. Stress strain and the crack spacing response of AR Glass fabric reinforced cement based composite

Figure 5.2 represents a picture of an AR Glass fabric cement specimen at two different strain stages of 0.9% and 2.5% strain. It can be seen that in between these strain ranges the number of parallel cracks have increased. A function representing

experimentally measured crack spacing is also shown in Figure 5.1 and indicates that it decreases as a function of applied strain.

Fig. 5.2. Glass Sample (a) At 0.9% strain (b) At 2.5% strain

Table 5.1 shows the set of samples selected for theoretical modeling. Glass and Polyethylene fabrics were used. Specific cases were selected to address the effect of fabric type and geometry, matrix formulations, and processing parameters so that the versatility of the model can be checked.

Table 5.1

Different Mix Properties

Mix ID	Mix Properties
A	No silica Fume, No Fly ash with Glass
B	40% Fly ash, No Silica Fume with Glass
C	No Silica Fume, No Flyash with glass and a pressure of 200 lbs
D	No Silica Fume, No Flyash with PE fabric

A close examination of the stress strain plots indicates that there are four distinct zones identified in the response of cement fabric composites with two zones prior to BOP and two zones after the BOP range. The behavior of the matrix and the fabric and their interaction is studied in each of these four ranges, and the formulations are compiled together to present a comprehensive material simulation model. The first two ranges correspond to the elastic-linear range and stable cracking-nonlinear range prior to the BOP point. The post BOP stage is characterized by formation of distributed cracking followed by a crack widening stage ultimately leading to failure. During the distributed crack formation, the crack spacing function continues to decrease. In the second stage of response, the crack spacing remains constant as the interface failure dominates the response. The strain imposed on the sample results in widening of the existing cracks. Since no new cracks are formed, response is dominated by the pullout slip of the fabric.

The material property data used in the modeling work were obtained from the uniaxial tension experiments as presented in Tables 5.2 and 5.3. The experimental data consist of a range of parameters in terms of the initial stiffness, cracked stiffness, BOP stress, BOP strain, ultimate strength capacity, and toughness. These experimental data are discussed in accordance to the material models obtained through the application of the theoretical model.

Mix	**$E_{initial}$ (MPa)**	**s_{BOP} (MPa)**	**e_{BOP} (%)**	**$E_{post-crack}$ (MPa)**
A	2045	1.22	0.057	290
B	4100	1.78	0.038	540
C	4425	3.47	0.098	819
D	1900	2.18	0.15	95

Tables 5.2 and 5.3

Different properties measured experimentally.

Mix	**$s_{ultimate}$ (MPa)**	**$e_{ultimate}$ (%)**	**Toughness Mpa**
A	14.36	4.93	0.462
B	23.79	4.83	0.848
C	23.50	2.77	0.40
D	7.96	3.74	0.23

5.2 Crack Spacing Evolution Law

In order to quantitatively analyze the cracking data presented in Figure 5.2, a procedure based on image analysis was developed to measure the crack spacing and its distribution. The procedure for data collection and analysis is discussed in detail in earlier publications by Mobasher, Pahilajani and Peled (2004) and Mobasher, Stang and Shah (1990). This automated approach results in a statistically sampled set of data collected at each strain level. A typical set of crack spacing measurements from images as shown in Figure 5.2 represents a general decrease in the spacing during loading until a saturation level is reached. This saturation level is indicated by the flattening of the crack spacing curve. Beyond this point, reduction in crack spacing is not observed, as further increase in the strain causes widening of existing cracks by fabric pullout. The saturation crack spacing in the specimen shown in Figure 5.1 is about 8 mm.

An empirically based damage evolution law was obtained from the experimental results of crack spacing as a function of applied strain. In this approach, an exponentially decaying function is used to parametrically express the experimental crack spacing versus strain profiles. A typical equation of crack spacing versus stain is given by,

$$S(e_i) = S_1 + S_0 e^{-a(e_i - e_{mu})} \qquad e_i > e_{mu} \tag{5.1}$$

Where, S = Crack Spacing.

ε_{mu} =strain at the BOP level, or where the first set of measurements were obtained

ε_i= independent parameter, strain at which the spacing is computed

S_0, α = constants representing the decay

S_1 = Saturation crack spacing

Typical values of S_1, S_0, ε_{mu} and α for different matrix and fabric combinations are given in Table 5.4. The numbers represent an average value of three replicate specimens tested under the same conditions. These parameters are used in the theoretical model to generate the crack spacing functions and constitute important properties that govern the cracking, debonding, as well as reduction of stiffness in the composite.

Table 5.4

Various Crack Spacing parameters used in the theoretical model

Mix	**S_1 (mm.)**	**S_0 (mm.)**	a	e_1
A	18	22	50	0.008
B	8	35	150	0.010
C	9	10	140	0.011
D	7	20	170	0.010

5.3 Theoretical Simulation of Fabric Pullout

In the third range of loading, the cross sections containing matrix cracks experience an additional load carrying component due to the fabric pullout. When the fabric is under load across an existing matrix crack, the stress is transferred into the matrix through the interfacial zone. The magnitude of the shear stress is a function of the

contact bond stiffness and the frictional properties between the two surfaces. Conceptually, the higher the bond, the higher tensile load can be resisted. A theoretical basis has been proposed to analyze the experimental results of fabric pullout from a cementitious matrix. The load transfer across a matrix crack can be calculated using a closed form fabric cement bond model by Sueki, Mobasher and Peled (2004). A model for pullout of straight yarns based on shear lag approach is used as the basis and the debonding growth and pullout under frictional and adhesion bond is modeled. The yarn model is capable of handling woven and bonded yarns using a periodic arrangement of linear springs providing anchorage at the warp/fill junctions. Anchorage at the point of intersection of yarns is attributed to the connection of the warp and fills yarns and the restraint offered by the fill yarns in redistributing the load. It may also be caused by the surface curvature of woven fabric. The simulation results have been compared with the experimental results of three fabric types: alkali-resistant glass (AR-glass), polypropylene (PP) and polyethylene (PE) and three different procedures for making samples (control, pultrusion, and vacuum). Model predictions verified the experimental results quite well. This theoretical procedure was used in order to characterize the pullout slip response of a fabric according to the de-bonded length, and the number of active junctions in redistributing the load. The general load slip relationship for a debonding fabric is expressed as:

$$P = P_y + P_d + P_b = t_f (2\pi r) L_d + \frac{-2\pi r t_{\max}}{b_2 \coth(b_2 (L - L_d))} + \sum_{i=1}^{n} K_b u(x_i) \tag{5.2}$$

$$U(L) = \frac{P - t_f L_d}{E_f \pi r^2 b_2} \coth\left(b_2 (L - L_d)\right) + \frac{P - \frac{1}{2} t_f L_d}{E_f \pi r^2} L_d \tag{5.3}$$

Where,

$$K_b = \frac{2k}{l} \frac{\sinh(l l) + \sin(l l)}{\cosh(l l) + \cos(l l) - 2} \qquad b_2 = \sqrt{\frac{G_i}{E_f \pi r^2}} \qquad l = \sqrt[4]{\frac{k}{4EI}} \tag{5.4}$$

Fiber-matrix interfacial shear stress, t, at the L_d is the length of debonding zone. $k = bk_0$. k_0 is the modulus of foundation in N/m^3, b is the constant width of the beam in contact with the foundation and EI is the flexural rigidity of the yarn treated as a beam. In the present approach, b is considered as thickness of yarn and I is calculated from fill-yarn geometry as done by Hetényi (1938). k_0 and E are considered as the values related to matrix and fiber interface. Note that the proposed methodology is capable of predicting the initial linear loading, partial debonding, and fabric pullout.

5.4 Formulation for a Single Lamina

A general approach for the treatment of cross ply laminate composites made with various fiber and matrix materials is used. The cross section of the specimen throughout its depth is divided into several layers and the stresses and strain within each layer are assumed to remain constant. The imposed strain field representing a constant for tension or compression field and linear function for a flexural mode is specified. As shown in Figure 5.3, each lamina is modeled as an orthotropic sheet in plane stress with direction

"1" representing the longitudinal direction of alignment of warp fibers, and direction 2 representing the transverse or fill direction. Parameters h_k and h_{k+1} represent the coordinates and top and bottom of lamina number "k" in a stack of "n" laminates.

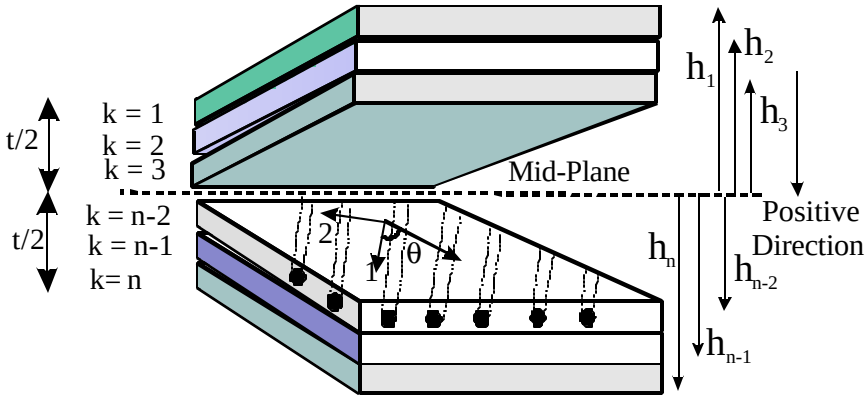

Fig. 5.3. Definition of lamina and coordinates used in generating stiffness coefficients.

The property of each layer is specified using the material properties and volume fraction of components. The fabric is assumed to be linear elastic, and its effect is incorporated in the properties of each lamina. Using the stacking sequence the overall axial and bending stiffness matrices are obtained. The equivalent elastic stiffness is obtained using the sum of the contributions from each layer to the overall value. Depending on the state of strain (normal and shear) and curvature distribution, strains at the top and bottom of the lamina are calculated and applied to the orthotropic model to identify the state of cracking and compute ply stress.

The model proposed for the stress-strain response of the matrix, fabric, and the composite is shown in Figure 5.5. In the elastic range the rule of mixtures for

longitudinal modulus and Halpin-Tsai estimates of transverse modulus were applied. Due to low volume fraction of fibers (normally less than 10%) the stiffness of the lamina is dominated by matrix properties. This zone is terminated by initial cracking of the matrix phase designated as σ_{t1}. After the initiation of cracks in the matrix, its load carrying capacity does not vanish as the cracks are bridged by the longitudinal yarns. The stiffness degrades up to the BOP level according to a single scalar damage parameter 'ω'. The form of the evolution of the damage parameter as a function of strain is expressed as a power law:

$$w = w_1 + a\,(e_i - e_{t1})^{b} \qquad e_{t1} < e_i < e_{mu} \tag{5.5}$$

The form of the function in Equation 1 was based on a model proposed by Karihaloo and Fu to formulate the damage vs. strain relationship. Stiffness in the cracked matrix decreases as the strain is increased. This is empirically based on a damage evolution model by Horii and Nemat Nasser and Hori. In this equation, the damage parameter ω?is calculated at various strain levels with constants α, β, and ω_1 as shown in the equation 5.5. The values of these constants are of α= 0.16, β= 2.3, and $\omega_1 = \varepsilon_{t1}$ H, where H is the gage length of the specimen used. σ_{t1} and $\varepsilon_{t1} = \sigma_{t1} / E_{m0}$ were used to represent the ultimate strength, and strain at failure under uniaxial tension for the paste in an unreinforced condition. The stiffness $E_m(\omega)$, defined as a function of damage and initial matrix elastic modulus E_{m0}:

$$E_m(w) = \frac{E_{m0}}{1+\frac{16}{3}w(1-u_m^2)} \tag{5.6}$$

This value of matrix stiffness is used in the rule of mixtures to obtain the longitudinal stiffness of the lamina $E_1(\omega)$, as defined in Equation 5.7. Calculation of the transverse modulus E_2 and ν_{12} were achieved using the Halpin-Tsai equations as shown in Equation 5.8. The value of ξ was set equal to 2 since the fabric used is circular.

$$E_1(w) = E_f V_f + E_m(w)(1-V_f) \tag{5.7}$$

$$E_2(w) = \frac{E_m(w)(1+x\ hV_f)}{1-hV_f} \qquad h = \frac{E_f - E_m(w)}{E_f + x\ E_m(w)} \tag{5.8}$$

The gradual decrease in the stiffness of the matrix starts at the plain matrix strength of σ_{t1} and according to Equation 5.9 the stress is computed using an incremental approach of adding the products of strain increments by the effective stiffness at that level. The stress in the matrix phase beyond the elastic range is calculated incrementally as:

$$s_1^i(w) = s_{t1} + \sum_{n=1}^{i} E_m(w)(e_n - e_{n-1}) \qquad e_i < e_{mu} \tag{5.9}$$

Deformations in Post Cracking Zone

The degraded stiffness at each strain value from ε_{t1} up to the BOP strain level (ε_{mu}) is computed and used to calculate the stress. The maximum damage level defined as ω_0, corresponds to the stress at the BOP level which is the ultimate strength of matrix in the presence of fibers σ_{mu}. The parameter ε_{mu} is obtained using the ACK approach which predicts the strain capacity of the matrix phase in the presence of fibers as shown in Equation 5.10. This approach has been verified to be applicable for the cement based

materials by showing that the strength of the matrix is increased in the presence of fibers. In this approach γ is the fracture toughness and r is the fiber radius. In the current study, γ = 0.5 N-mm has been used, resulting in a good correlation between experimental and theoretical results.

$$e_{mu} = \left[\frac{12 t g_m E_f V_f^2}{E_c E_m^2 r V_m} \right]^{\frac{1}{3}} \tag{5.10}$$

Beyond the BOP level, the response is dominated by initiation of parallel microcracking in the matrix phase. The gradual reduction of matrix stress levels in the vicinity of the cracked matrix is referred to as the softening zone. In this zone the matrix cracks widen and while there may be no localization, the strain softening region is defined as a zone where the response is governed by a smeared crack model with contributions from a softening matrix and the fabric pullout force. The matrix stress capacity is assumed to an exponentially decaying function of the maximum stress. The stress in the strain-softening zone asymptotically approaches zero, after which the model is comparable to the ply discount method. The choice of the exponent parameter affects the rate of drop of the stress as a function of strain. This response is modeled as

$$s_1^i(w) = s_{mu} e^{-(e_i - e_{mu})w} \qquad e_i > e_{mu} \tag{5.11}$$

Where, "w" represents the exponent coefficient affecting the rate of decay in stress from the peak composite stress. The range of values of w=50-150 was used in the simulation of the data in this study. The definition of strain in this region is gage length dependent and the present approach uses the mean strain over the length of several cracks in the matrix. As the specimen undergoes strain softening, an exponential decaying

stiffness similar to Equation 5.7 utilizing the stiffness at peak was used. The modulus E_m, computed for each strain level ε_i, was proportional to the reduction of the stress from the peak value using Equation 5.7.

A parametric study of the relationship between the crack spacing and the changes in the stiffness degradation is shown for two fiber systems according to Figure 5.4. In this plot experimental data for crack spacing and also tangent stiffness at various strain levels are plotted at various strain levels for two fabric system. It is noted that through the elimination of strain as the independent variable, a good correlation between these independent measurements of damage are obtained.

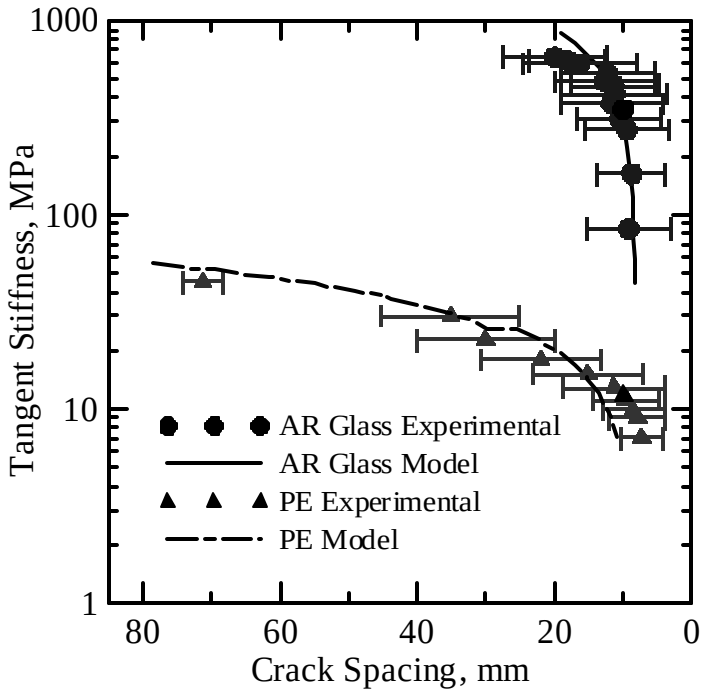

Fig. 5.4. Parametric study for glass and polyethylene systems.

The displacement of the specimen is obtained by integrating the strain components in the uncracked segments and adding it to the slip parameters obtained from

the cracked regions. The crack spacing parameter determines the multiple number of sections which should be taken into account in the calculations of displacements. The applied slip under a given load is adjusted for a factor of 2 to represent crack opening across each crack face. This displacement is added to the displacement obtained through the uncracked segments assumed to carry an average strain of ε_{mu}. Subsequent loadings of a cracked layer results in a change in the magnitude of the crack spacing as obtained from the damage evolution law. The response of a matrix in the strain-softening zone asymptotically approached to a level of zero stress. Function C (P) represents the compliance of the debonded fabric as a function of applied load and is obtained from the pullout load slip response defined using equations 5.2 and 5.3.

$$\Delta(e_i) = \left[e_{mu} + 2P(e_i)\frac{1}{S(e_i)}C(P) \right] H \quad e_i > e_{mu} \tag{5.12}$$

In this equation H represent the gage length, $P(\varepsilon_i)$ and $S(\varepsilon_i)$ represents the load and crack spacing at each strain level. This approach assumes that at any stress level, the degradation of elastic properties is primarily related to the magnitude of crack spacing and overall strain response. Using the updated damage, the quasi-elastic stiffness parameters are obtained and used to calculate the load and moment for that increment.

Formulation for a Laminate in Tension, Shear or Flexure

Depending on the state of normal strain in each lamina, the stiffness is calculated incrementally and applied to the orthotropic model to calculate the stress in each ply. Due to the incremental nature of the solution, no load redistributions are considered. The constitutive relations for a general orthotropic material include the stiffness matrix, *A*, and relate the stress and strain within a lamina loaded in its principal directions. The

stiffness of the matrix due to cracking is updated with each increment of applied strain. An elastically equivalent compliance matrix is defined with the updated elastic properties.

$$\Delta e^{i}_{j} = \overline{S}^{i}_{jk}\ \Delta s^{i}_{k}$$
$$s^{i}_{k} = \left(\overline{S}^{i}_{jk}\right)^{-1} \Delta e^{i}_{j} + s^{i-1}_{k} \tag{5.13}$$

Or in form:

$$\overline{S}_{11} = \frac{1}{E_{1(w)}} \qquad \overline{S}_{12} = -\frac{u_{12}}{E_{1(w)}} \qquad \overline{S}_{22} = \frac{1}{E_{2(w)}} \qquad \overline{S}_{66} = \frac{1}{G_{12(w)}} \tag{5.14}$$

By inverting the compliance matrix, S, the stiffness matrix *A* is obtained which relates the strains into stresses for each lamina loaded in principal material direction

$$\overline{A}_{ij} = \sum_{m=1}^{n} \left(\overline{S}^{i}_{jk}\right)^{-1} (h_m - h_{m-1}) \tag{5.15}$$

The form of sub matrix "A" is discussed by Jones (1975), and represents the extensional stiffness and "N" the force per unit length of cross section. With knowledge of strain the stress distribution per lamina is computed for each loading step in an incremental fashion. The strains and forces were updated incrementally according to the matrix form representation:

$$\left[\Delta N\right] = \left[\overline{A}(w)\right]\ \left[\Delta e\right] \tag{5.16}$$

$\overline{A}$ takes into account the fact that some of the layers have cracked, softened, or fractured, and the tangent stiffness of the material is used in calculation of these stiffness coefficients. After each iteration, the incremental loads and strains are determined and the results are added to the loads and strains at the previous ply failure. The applied load at the i^{th} interval was represented as N_i according to:

$$N_i = N_{i-1} + \Delta N_i = N_{i-1} + \left[\overline{A}(w)\right]_i\ \left[\Delta e_i\right] \tag{5.17}$$

The incremental algorithm for calculation of load deformation in the axial response is as follows: the geometrical dimensions of the lamina and the stacking sequence are defined. Depending on the nature of loading in terms of uniaxial or biaxial tension or compression, the strain distribution is calculated and imposed incrementally. At each increment of the strain, the stiffness coefficients of matrix A, are calculated and used to obtain the stress at that increment. Before advancing to the next loading increment, the stresses are checked against the failure criterion, and if it is met, then the stress level and the stiffness of that particular layer are adjusted according to the constitutive response. The material properties are updated for subsequent analysis.

Analysis of the Results

A parametric study was conducted to show the sensitivity of the model to the range of the parameters studied. Several parameters were evaluated which include the stiffness of the fabric material, the fabric volume fraction, and the effect of the bond strength of the fabric and cement paste.

Figure 5.5 represents the behavior of the model with varying volume fraction of the fabric material. Note that as the fabric volume fraction increases, the stiffness of the composite in the post cracking range increases as well. The effect of stiffness of the fabric on the overall stress strain response of the composite is shown in Figure 5.6. Note that increasing the stiffness of the fabric material has a direct effect on the overall stiffness characteristics of the system, and allows faster transfer of load back into matrix.

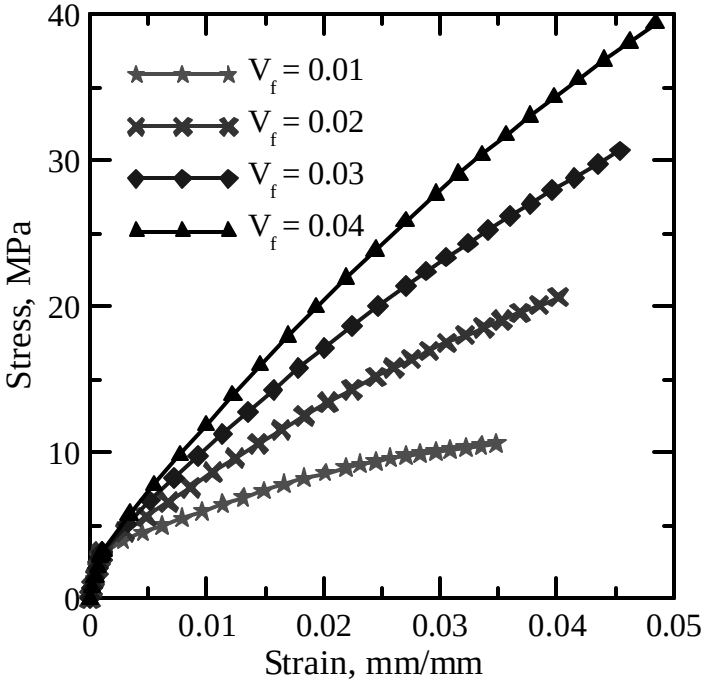

Fig. 5.5. Graph showing the behavior of the model with varying volume fraction.

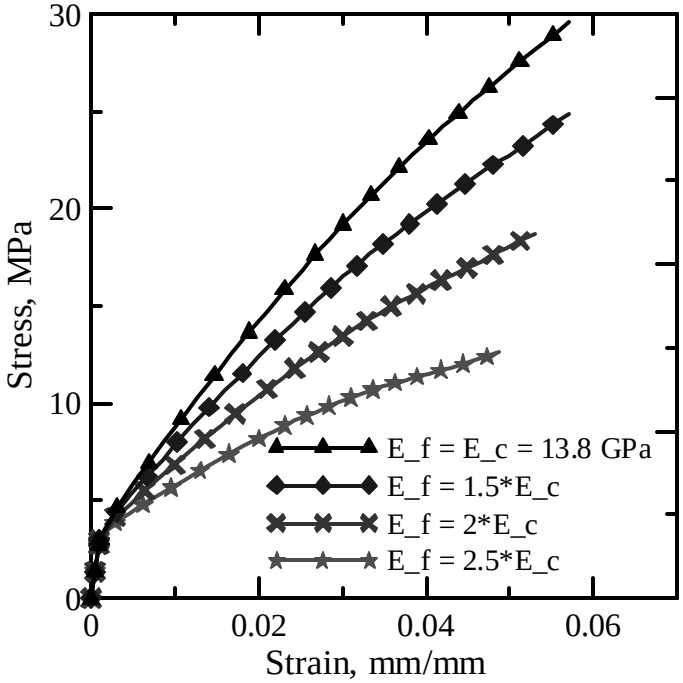

Fig. 5.6. Graph showing the behavior of the model with varying stiffness values of the AR Glass fabric.

A parametric study is also shown to show the effect of overall stiffness of the interface on the crack spacing response. When the bond is weak, pullout of the fabric takes place at the expense of additional cracking. It is shown that the dominant mode of failure changes from distributed cracking to crack widening according to Figure 5.7. Note the crack widening results in a higher loss of stiffness as compared to parallel crack formation. In order to make this simulation possible, only the interface shear strength (τ) of the composites were used, and the resulting pullout response was used in the analysis of the tensile test data, according to Equation 5.12.

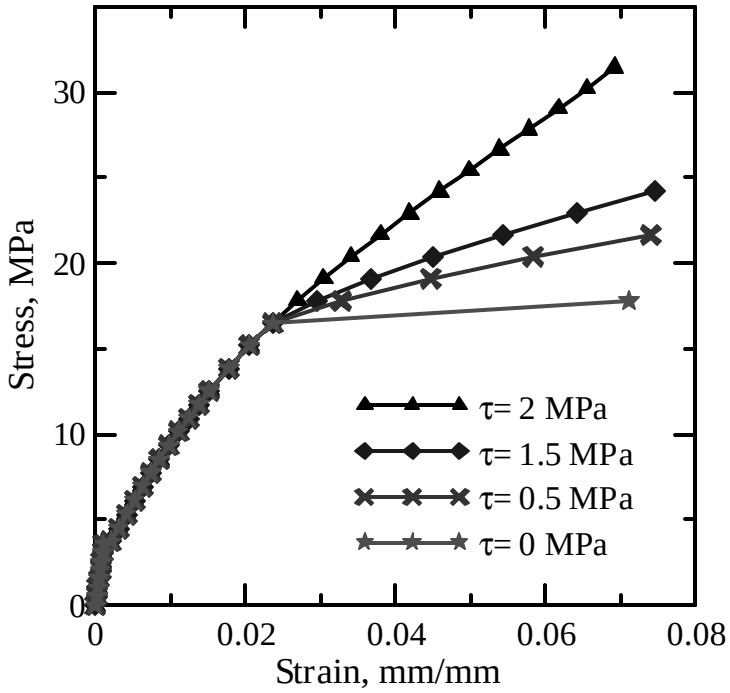

Fig. 5.7. Graph showing the behavior of the model with varying values of bond strength of the AR Glass fabric.

Comparison with Experimental Results

Components of the model were tested with the results of stress strain and crack spacing – vs. strain response of the composites. Several case studies were used. The first case study was involving glass fabrics with 40% flyash level. A simulation was carried out using the parameters presented in the table 5.4. The experimental stress strain response with the model predictions are shown in figure 5.8. The crack spacing versus strain response obtained experimentally as well as theoretically is show in the same figure. The model gives a good prediction of both responses.

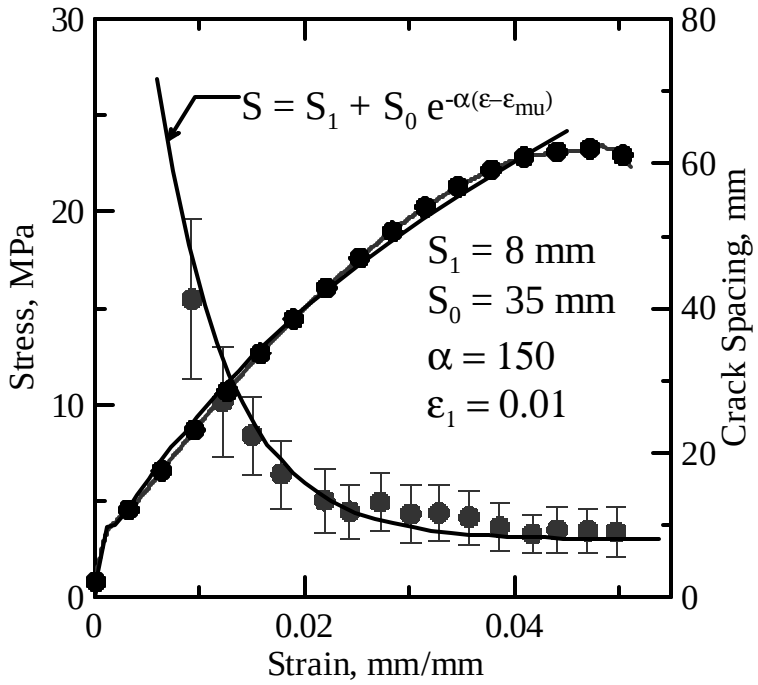

Fig. 5.8. Stress and crack spacing plots plotted versus strain for a sample with Glass fabric (40% flyash) along with the theoretical model response which gives the fit for the crack spacing and the stress strain response.

To check the accuracy of the model with a different fabric system, a similar study was carried out using the Polyethylene (PE) fabrics. Figure 5.9 shows two replicate samples of Polyethylene cement composites along with the model response. Note that both the stress-strain and the crack spacing response of replicate samples are sufficiently close to the theoretical simulations.

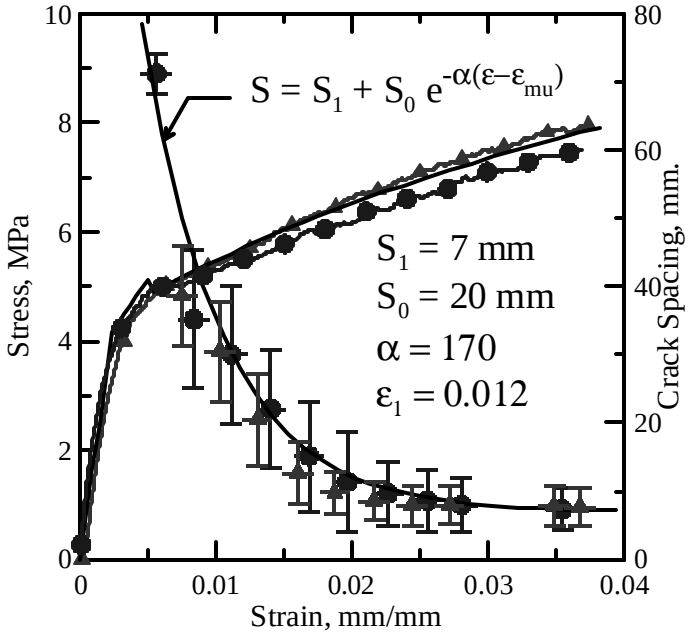

Fig. 5.9. Stress and crack spacing plots plotted versus strain for 2 samples with poly-ethylene fabric along with the theoretical model response which gives the fit for the crack spacing and the stress strain response.

Effect of changes in matrix formulation of the composite response is shown with the AR Glass fabric but with two different matrix properties. Effect of replacement of Portland cement with as much as 40% flyash is studied in Figure 5.10. The bond parameters are affected by the use of flyash, resulting in an increase in the interfacial

strength. This parameter affects the overall response of the system, and the crack spacing parameters. A bond strength of 1.6 MPa was used for the matrix with 40% flyash as compared to a shear strength of 1.2 MPa used for the control sample. The model is capable to using the interface parameters shows how the model can be used for different fabrics and matrix properties.

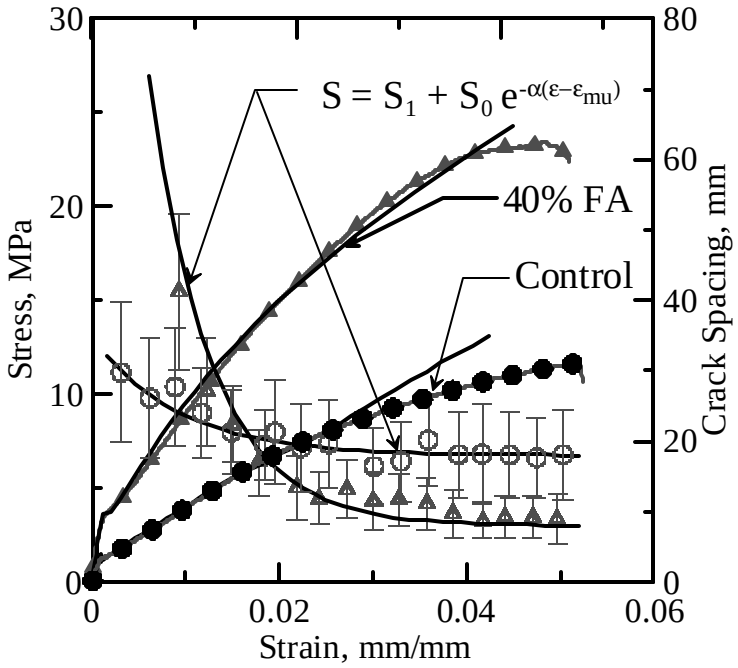

Fig. 5.10. Stress and crack spacing plots plotted versus strain for samples with glass fabric (with and without flyash) along with the theoretical model.

The bonding in the case of high flyash content matrix is high due to the better penetration of the fine flyash particles. The voids within the matrix as well as the interface of the matrix and fabric are filled, and the amount of calcium hydroxide at the interface is reduced considerably. Therefore, when we look at the stress strain response of these two systems (one with flyash and one without it), the cracking stage is predominant

in the former while in the latter crack widening is initiated at a very early stage. SEM photographs of the system with high flyash content are shown in figure 5.11. It shows how the flyash particles have more penetrability in the voids supporting a better bond.

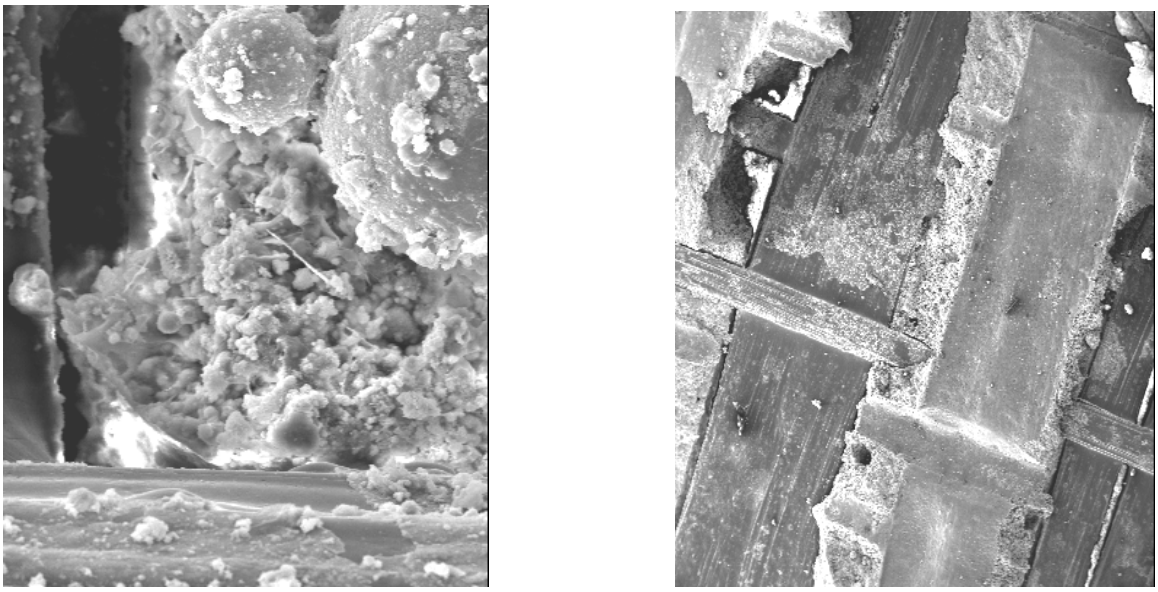

Fig. 5.11. SEM image of sample with 40% flyash showing the flyash particles: (a) occupying the voids (b) covering the surface of the fabric even after failure.

The last case study was to evaluate the effect of pressure applied during casting of the specimen. It has been shown that application of pressure results in better bonding and improvements in the characteristic bond development between the fabric and the cement paste. This has been verified using the crack spacing measurements as well. During the forming process, two different pressure levels of 1.7 kPa and 15 kPa were applied on top of the laminates to study the effect of penetration of the matrix in between the opening of the fabrics.

Figure 5.12 presents the effect of the applied pressure on the tensile response as well as crack density. It is clearly shown that the initial cracking stress, the post crack stiffness, the ultimate strength, and also the mean crack density are all dependant on the level of applied pressure. An increase in the pressure increases the tensile strength of the composite by about 40%, and the saturation crack density decreases suggesting better bonding and improved mechanical behavior.

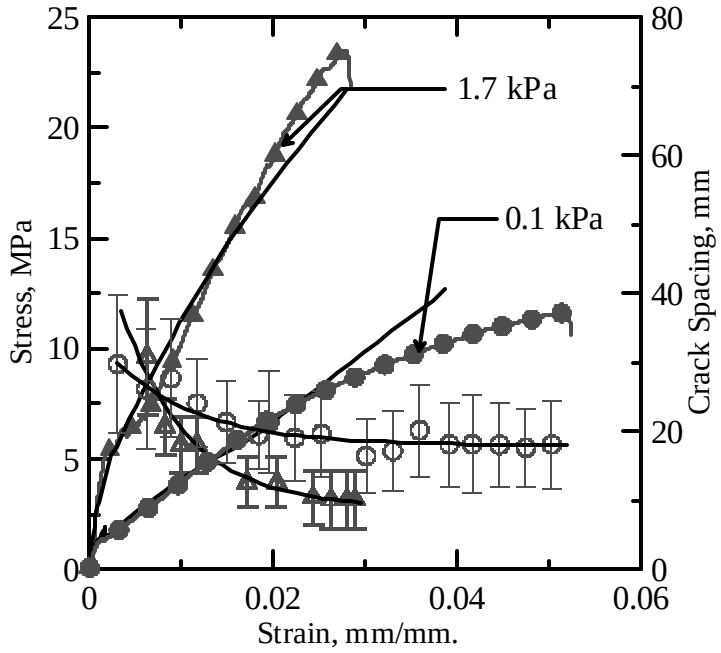

Fig. 5.12. Stress and crack spacing plots plotted versus strain for samples with glass fabric (with and without pressure) along with the theoretical model.

CHAPTER 6

CONCLUSION

The first part of this study primarily focuses on understanding the mechanical performance of fabric reinforced composite materials with various fabric and mix types. The second part is the study of the effects of mineral admixtures on the composites with AR glass fabric composites as the fabric. The final focus is on the theoretical modeling aspect of the fabric reinforced composites.

Experimental

It has been shown that through addressing the processing and material properties, novel manufacturing technique of pultrusion can be used to manufacture fabric reinforced cement based system with properties superior to other cement based composite systems. A comparative study of these different fabrics as affected by various process parameters indicates that the best mechanical behavior was achieved for glass fabric composites when high content of fly ash was replaced with the cement at the rate of 60% by volume. The mechanical properties of high content fly ash composite were highly influenced by the curing process used, perhaps due to the direct effect on the bond development. When the composite was cured for 28 days, a stiff composite was obtained with well distribution of the cracks.

The primary mechanism of the PE composite was found to be crack widening by fabric pullout, whereas in the glass fabric composites, crack widening was not the governing mechanism until 80% of the strain capacity was reached. It was only during

the final phase of loading where no new cracks are developed and the fabric begins to pullout from the matrix. This was evaluated by comparison of the crack spacing strain responses of both composites, suggesting that the glass fabric is well bonded to the matrix and the tensile behavior is well representative of the entire composite. Moreover, the samples with glass fabrics show a stiffer response in the post crack stress strain relationship than PE fabrics. While the stiffness reduction in glass is very high, it is seen that the tangent stiffness of PE at the post-cracked stage is quite lower than glass. The intensity of the static pressure applied after casting affects the mechanical behavior of the pultruded composites. Increasing the pressure improves the tensile strength due to improvement in bond strength, as suggested by the significantly higher crack density of the composite with the high pressure (15.3 KPa), suggesting better bonding and improved mechanical behavior of the high-pressured composite.

PP and PVA have shown similar trends as PE but the strength and toughness are highest in the case of PP fabric. The strength achieved is higher than glass and unlike glass PP does not show brittle failure. The PP and PVA fabrics have significant number of cracks and they also have a relatively small crack widening phase.

The main results from the experiments are summarized below.

a. Different fabric types have different effects. AR-glass fabric increased the strength of composite material; however, PE increased the toughness.
b. Woven fiber provides higher interfacial bonding than unidirectional yarn. This is caused by the restraint of fill yarns.

c. Different procedures (cast and pultrusion) used in making the specimen caused significant differences in results depending on the fabric type (AR-glass, PP, PE and PVA). When pultrusion bath was used, cement adsorption and penetration increased. As a result, maximum load also increased, specially, for the fabric that did not have coating around.

d. The addition of fly ash in cement mix increased the maximum load and interfacial shear bond. This supports the previous study done by Peled and Mobasher (2003) where they found the fabric reinforced concrete when mixed with fly ash increased tensile strength and toughness.

Theoretical Model

A procedure is presented to relate the damage evolution in the fabric reinforced cement based composites to the mechanical response. The crack evolution and the stiffness degradation can be related to the applied strain, and using composite laminate theory and incremental approach is developed to model the uniaxial tensile response of the composites. Test results are studied by means of parametric study and various experimental observations are explained using the simulation technique. The model is good way to predict the behavior of composites and can be used to replace the testing with further improvement. Right now it is limited to the case where the number of layers of fabric is 8. modifications from 8 layers to lesser number of layers can be done by putting the volume fraction as zero in the layers where there is no fabric.

Further Work

Experimental: Data obtained in this thesis are valuable to understand the use of fabrics (glass, PP, PE and PVA) with cement concrete as a composite construction material. However, we can achieve further improvement by extending more work in future.

a. Tensile tests are only one part of the test conditions. The next logical step would be to implement the pullout model into these different tests like flexural and bond.
b. The study can be further extended to studying hybrid composites. Such composites will have the advantages of two or more fabric types and will produce better results.
c. Furthermore, use of additives that enhance the early strength gain of flyash based composites will also help us overcome the problem inherited due to the addition of flyash.

Theoretical Model: To understand the response of fiber reinforced composite material, this study is valuable. However, this work can be extended for further understanding in future work.

a. The model can be converted to simulate the flexural tests. If the model incorporates both the tension and the flexure response its versatility will increase and it will become more efficient.
b. As more and more experimental data is generated one can take the model to deal with different orientation of fabrics and hybrid composites. If the parameters that will run these conditions are obtained the use of the model will greatly increase.

REFERENCES

Agarwal, Bhagwan D., and Lawrence J. Broutman. Analysis and Performance of Fiber Composite. New York: Wiley-Interscience Publication, 1990.

Allen, D. H., C. E. Harris, and S. E. Groves. "A Thermomechanical Constitutive Theory For Elastic Composites with Distributed Damage – I. Theoretical Development." International Journal of Solids and Structures. 23 (1987) 1301-18.

Allen, D. H., C. E. Harris, and S. E. Groves. "A Thermomechanical Constitutive Theory For Elastic Composites with Distributed Damage – II. Application to Matrix Cracking in Laminated Composites." International Journal of Solids and Structures. 23 (1987) 1319-38.

Aveston, J., and A. Kelly. "Theory of Multiple Fracture of Fibrous Composites." Journal of Materials Science. 8 (1973) 352-62.

Greszczuk, L. B. "Theoretical Studies of the Mechanics of the Fiber-Matrix Interface in Composites" ASTM STP 452, American Society for Testing and Materials. (1969) 42-58.

Gurney, C., and J. Hunt. "Quasi-Static Crack Propagation." Proceedings of the Royal Society of London Series A – Mathematical and Physical Sciences. 299 (1967) 508-24

Haupt, Garrett James. Study of Cement Based Composites Manufactured by Extrusion, Compression molding and Filament Winding. MS Thesis. Tempe: Arizona State University, 1997

Hetényi, M. Beam on Elastic Foundation. Ann Arbor: University of Michigan Press, 1983.

Hull, Derek. An introduction to composite materials. New York: Cambridge University Press, 1981.

Jones, Robert M. Mechanics of Composites Materials. 2nd ed. Philadelphia: Taylor & Francis, 1999.

Kelly, A., and W. R. Tyson. "Fiber-Strengthened Materials." High-Strength Materials ; Proceedings of the Second Berkeley International Materials Conference: High-Strength Materials – Present Status and Anticipated Developments. Held at the University of California, Berkeley, June 15-18, 1964. Ed. Victor F. Zackay. 1965. 578-602.

Lawrence, P. J. "Some Theoretical Considerations of Fiber Pull-Out from an Elastic Matrix." Journal of Material Schience. 7 (1972) 1-6.

Mobasher, B., and Cheng Yu Li. "Effect of Interfacial Properties on the Crack Propagation in Cementitious Composites." Journal of Advanced Cement Based Materials. 4 (1996): 93-105.

Mobasher, B., D. Kingsbury, J. Montesinos, and R. S. Gorur. "Mechanical Aspects of Crimped Glass Reinforced Plastic (GRP) Rods." IEEE Transactions on Power Delivery. 18 (2003): 852-8.

Peled, A., A. Benture, and D. Yankelevsky. "Woven Fabric Reinforcement of Concrete Matrix." Journal of Advanced Cement Based Materials. 1 (1994): 216-23.

Peled, Alva, and Barzin Mobasher. "The Pultrusion Technology for the Production of Fabric-Cement Composites." Brittle Matrix Composites 7 – Proceedings of the 7th International Symposium. Ed. Brandt, A. M., V. C. Li, and I. H. Marshall.

Cambridge: Woodhead Publ. Ltd.; Warsaw: ZTUREK Research-Scientific Institute, 2003. 505-14.

Stang, H., Z. Li, and S. P. Shah. "Pullout Problem: Stress Versus Fracture Mechanical Approach." Journal of Engineering Mechanics. 116 (1990): 2136-50.

Talreja, R. "Stiffness Properties of Composite Laminates with Matrix Cracking and Interior Delamination." Engineering Fracture Mechnics. 25 (1986): 751-62.

Peled, Alva, Barzin Mobasher and Pahilajani Jitendra. "Pultrusion of Fabric Reinforced High Flyash Blended Cement Composites." Manuscript in review.

Peled, Alva, Barzin Mobasher and Pahilajani Jitendra. "Damage Evolution in Fabric-Cement Composites." Manuscript in review.

Peled, Alva, Barzin Mobasher and Pahilajani Jitendra. "Modeling of Fabric Reinforced Cement Based Composites." Manuscript in review.

APPENDIX A

GRAPHS FOR ALL THE TESTED SAMPLES (7 Days)

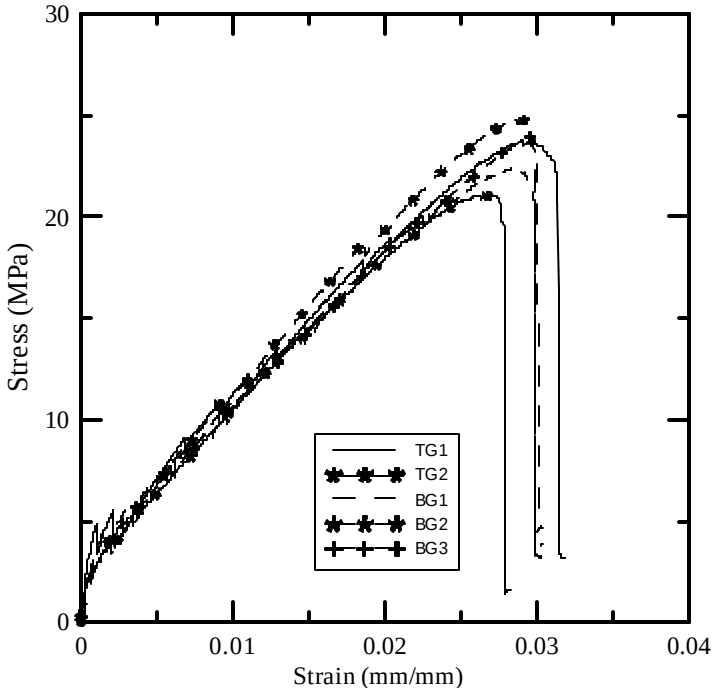

Fig. A-1. AR-glass fiber samples with matrix #5

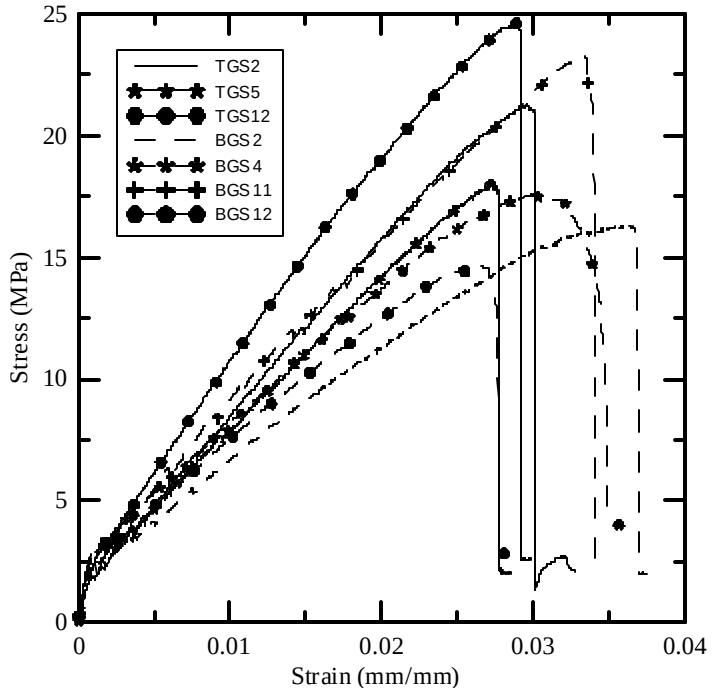

Fig. A-2. AR-glass fiber samples with matrix #2

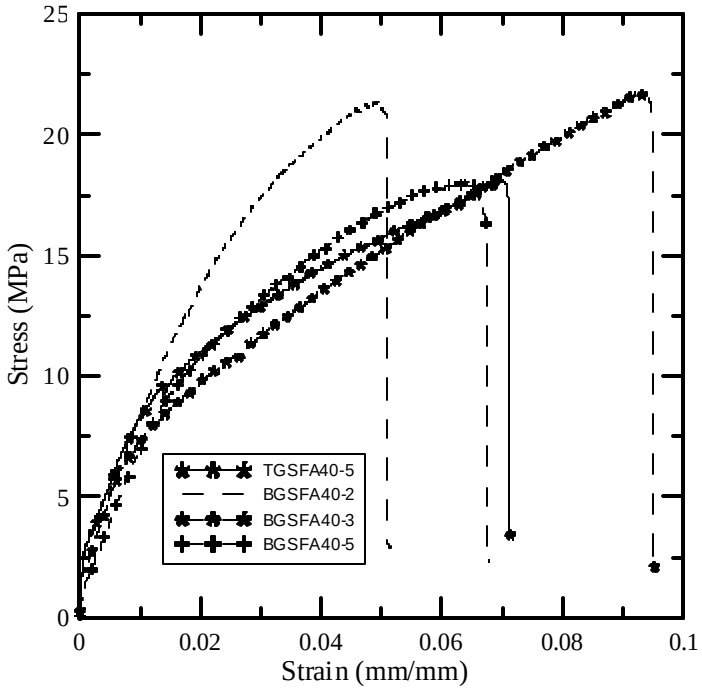

Fig. A-3. AR-glass fiber samples with 40% Flyash content and 5% Silica Fume

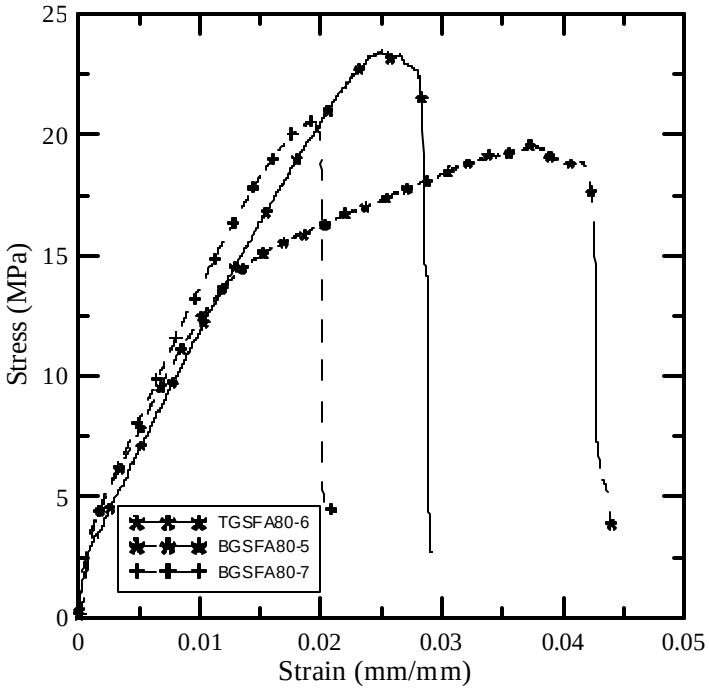

Fig. A-4. AR-glass fiber samples with 80% Flyash content and 5% Silica Fume

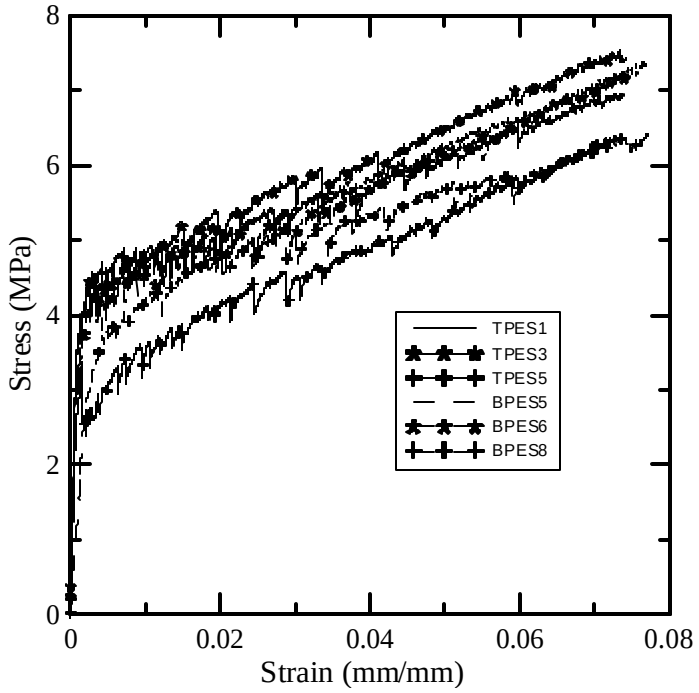

Fig. A-5. PE fiber samples with matrix #2

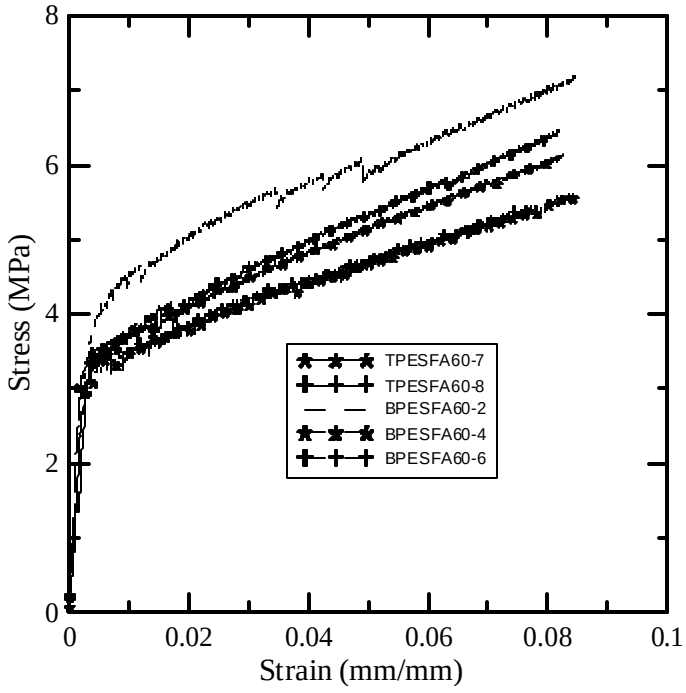

Fig. A-6. PE fiber samples with 60% Flyash content and 5% Silica Fume

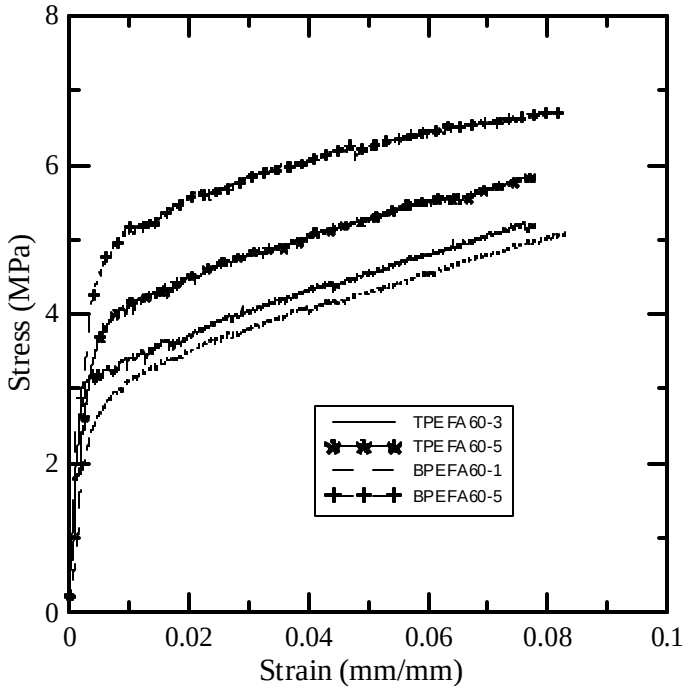

Fig. A-7. PE fiber samples with 60% Flyash content

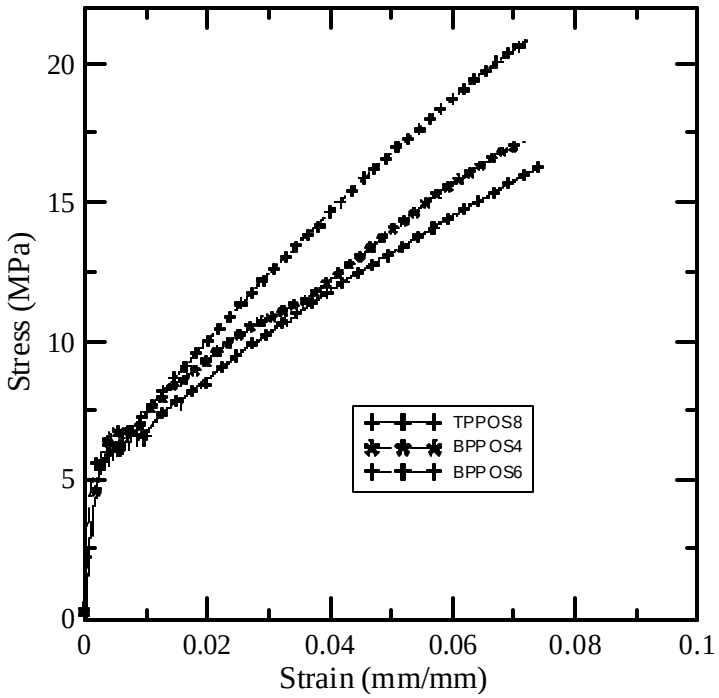

Fig. A-8. PP fiber samples with Matrix#2 and cast in opposite direction of fabric

APPENDIX B

GRAPHS FOR ALL THE TESTED SAMPLES (28 Days)

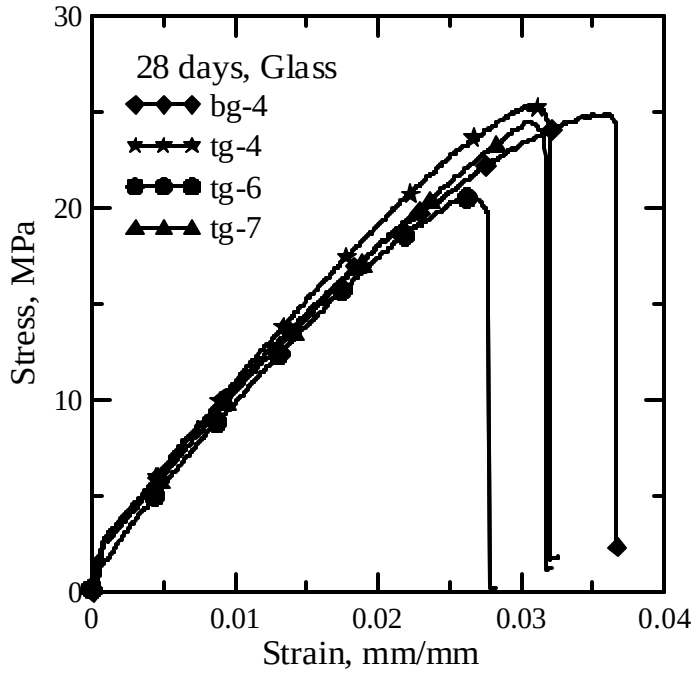

Fig. B-1. AR-glass fiber samples with matrix #5

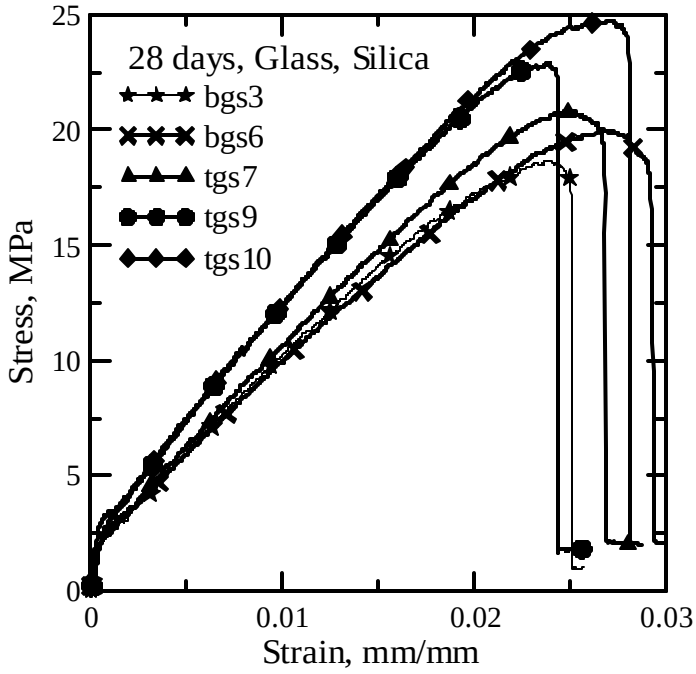

Fig. B-2. AR-glass fiber samples with matrix #2

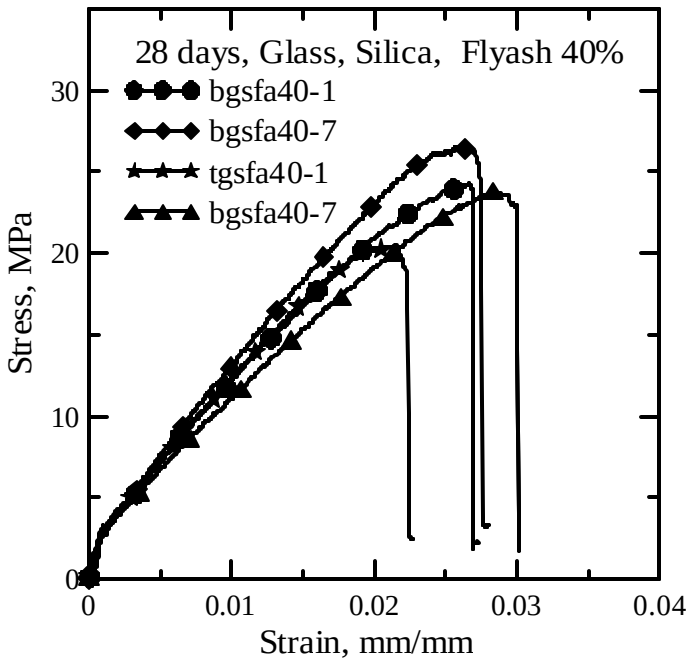

Fig. B-3. AR-glass fiber samples with 40% Flyash content and 5% Silica Fume

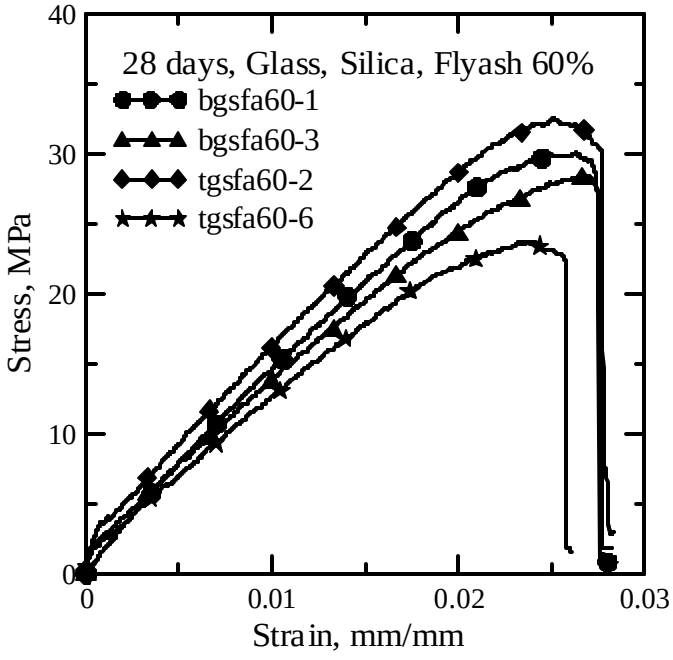

Fig. B-4. AR-glass fiber samples with 60% Flyash content and 5% Silica Fume

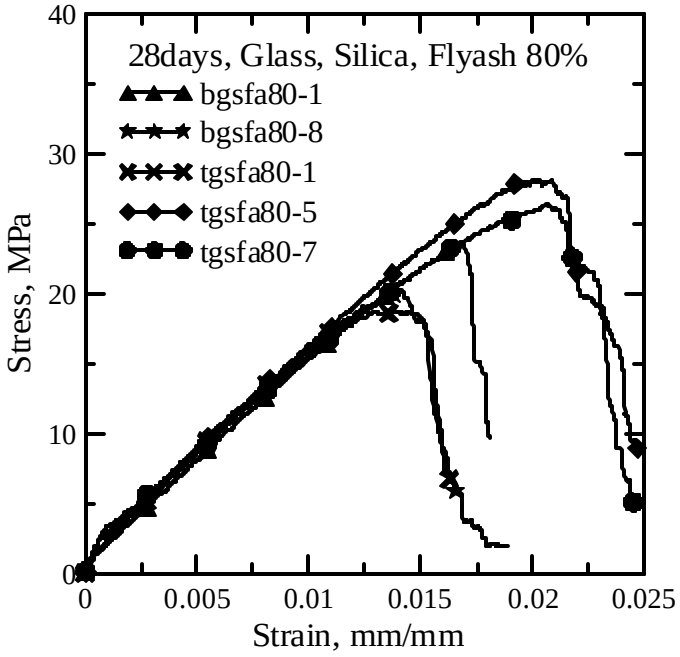

Fig. B-5. AR-glass fiber samples with 80% Flyash content and 5% Silica Fume

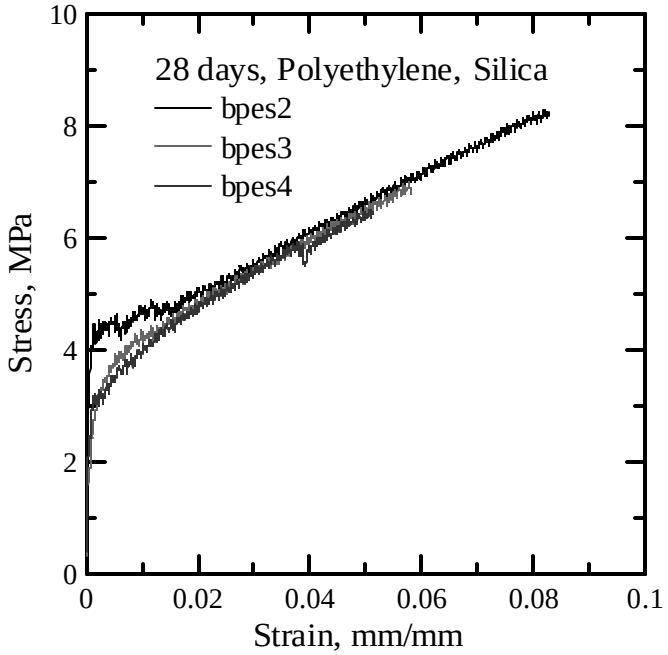

Fig. B-6. PE fiber samples with matrix #2

APPENDIX C

GRAPHS FOR COMPARISONS

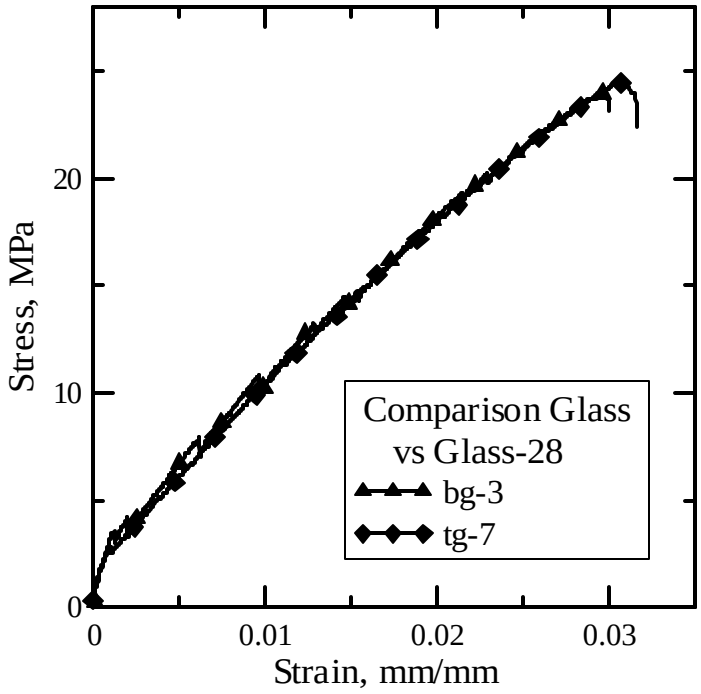

Fig. C-1. Comparison of AR-glass fiber samples with matrix #5 at 7 and 28 days

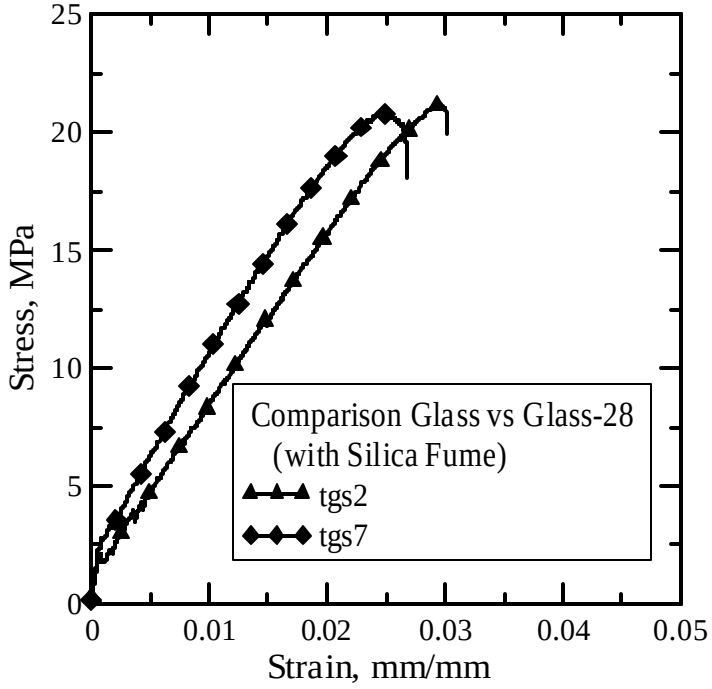

Fig. C-2. Comparison of AR-glass fiber samples with matrix #2 at 7 and 28 days

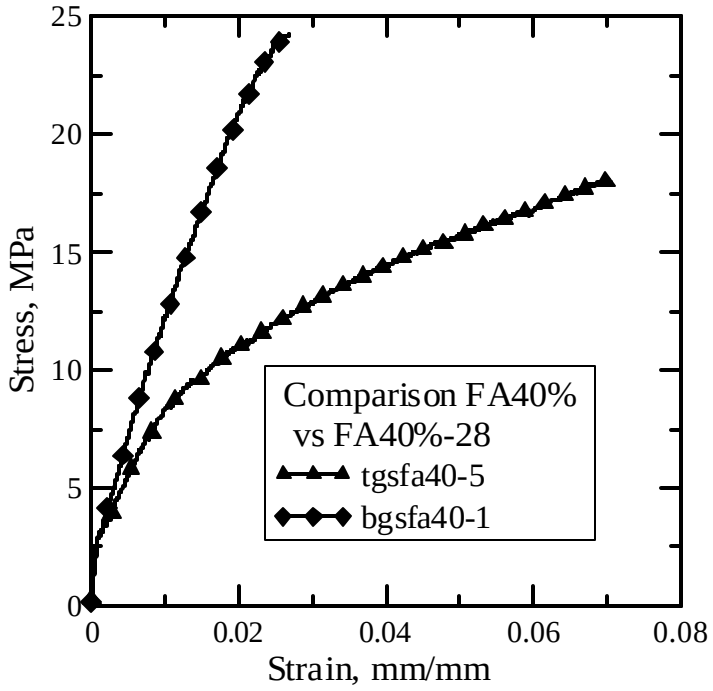

Fig. C-3. Comparison of AR-glass fiber samples with 40% Flyash at 7 and 28 days

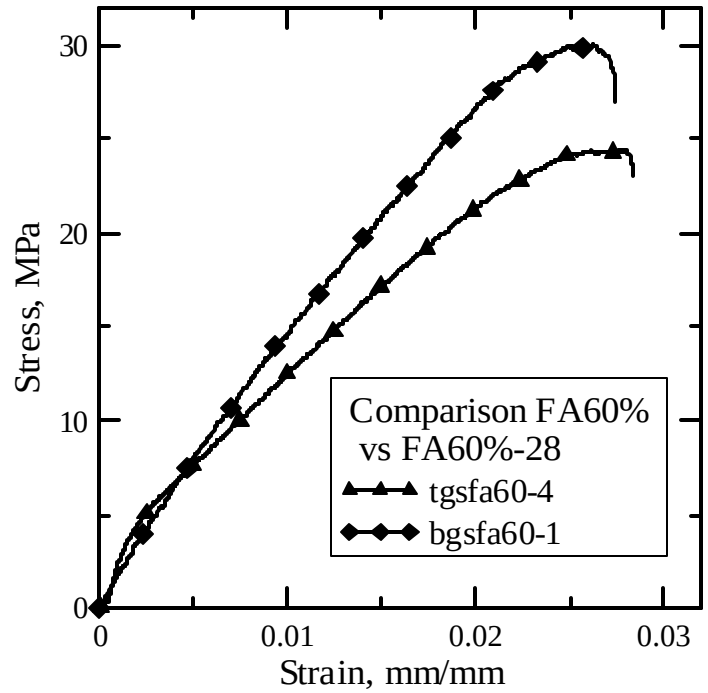

Fig. C-4. Comparison of AR-glass fiber samples with 60% Flyash at 7 and 28 days

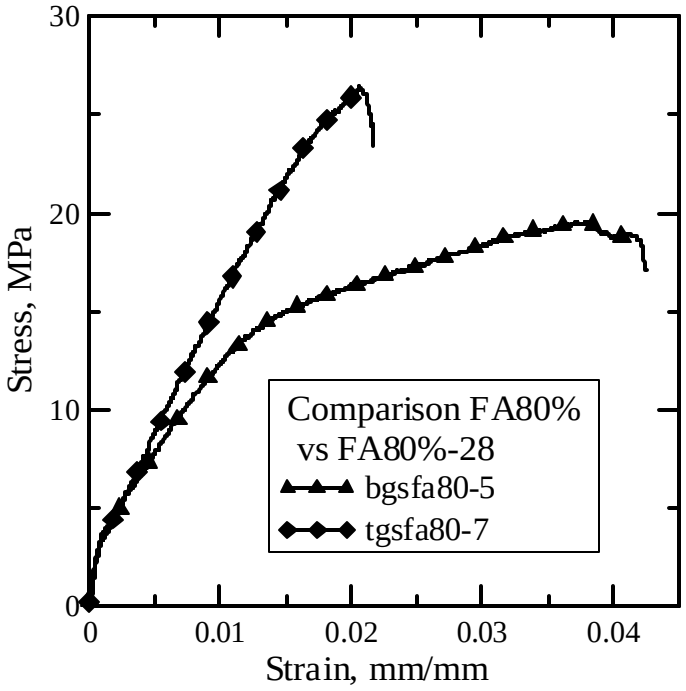

Fig. C-5. Comparison of AR-glass fiber samples with 80% Flyash at 7 and 28 days

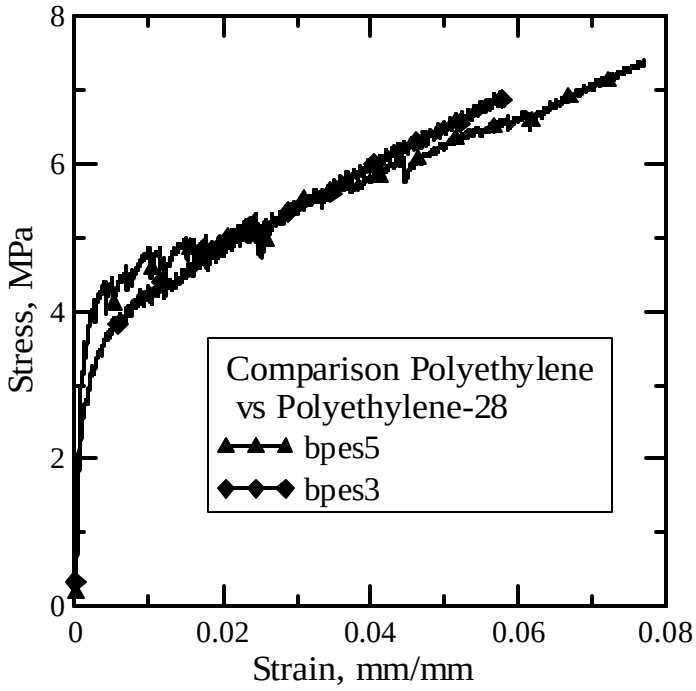

Fig. C-6. Comparison of PE fiber samples with matrix#2 at 7 and 28 days

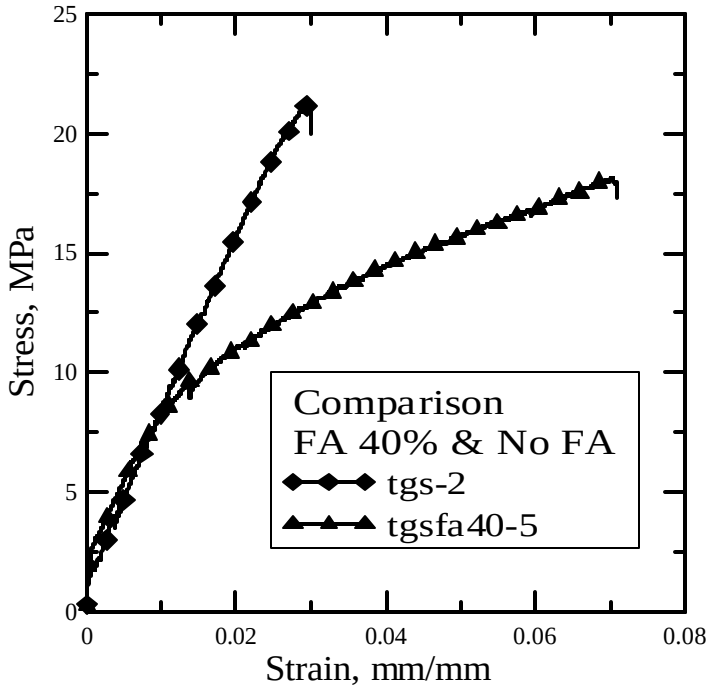

Fig. C-7. Comparison of AR-glass fiber samples with 40% FA and 0% FA (5% SF)

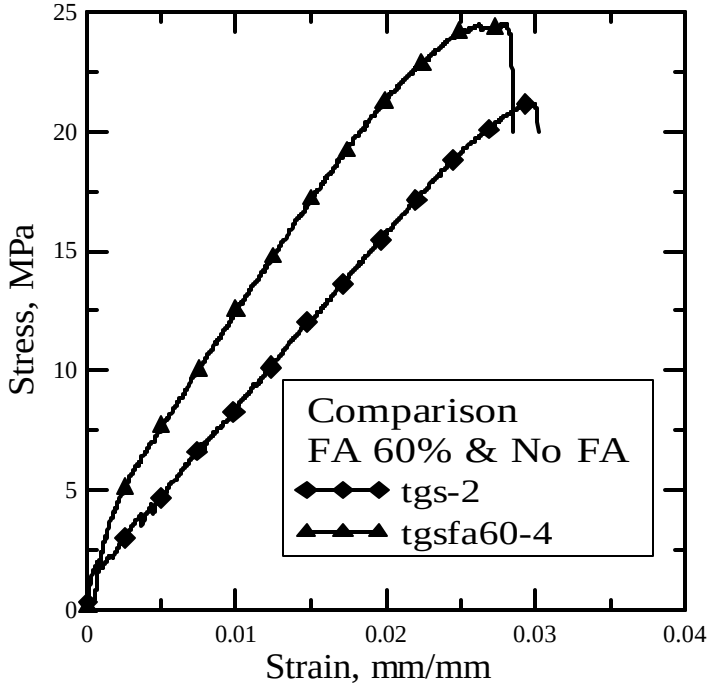

Fig. C-8. Comparison of AR-glass fiber samples with 60% FA and 0% FA (5% SF)

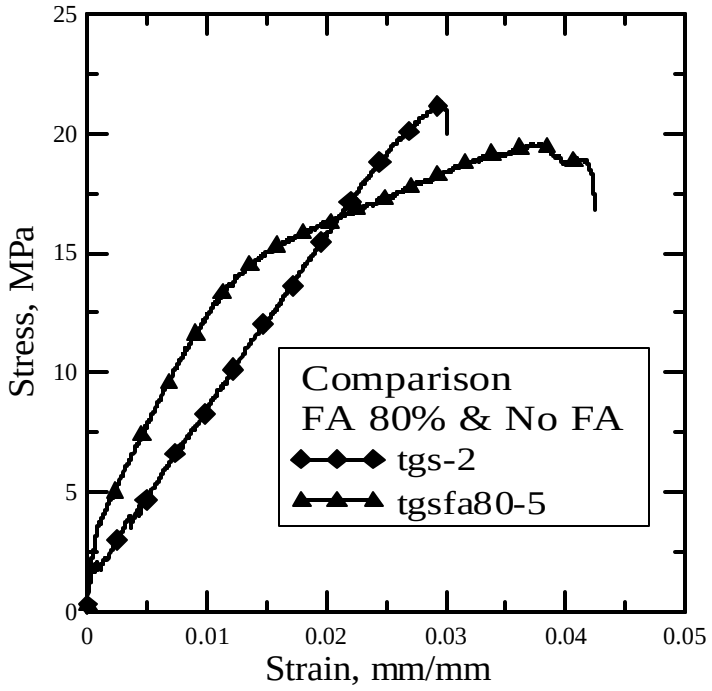

Fig. C-9. Comparison of AR-glass fiber samples with 80% FA and 0% FA (5% SF)

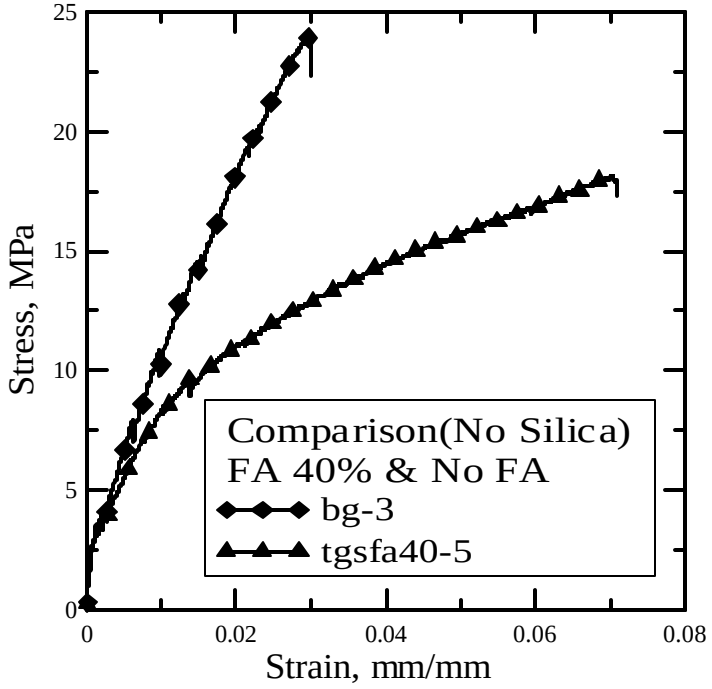

Fig. C-10. Comparison of AR-glass fiber samples with 40% FA and 0% FA (No SF)

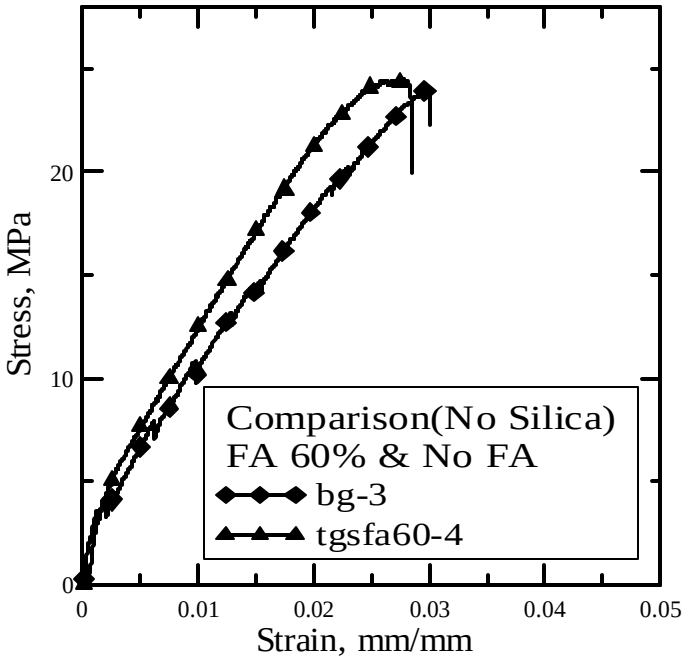

Fig. C-11. Comparison of AR-glass fiber samples with 60% FA and 0% FA (No SF)

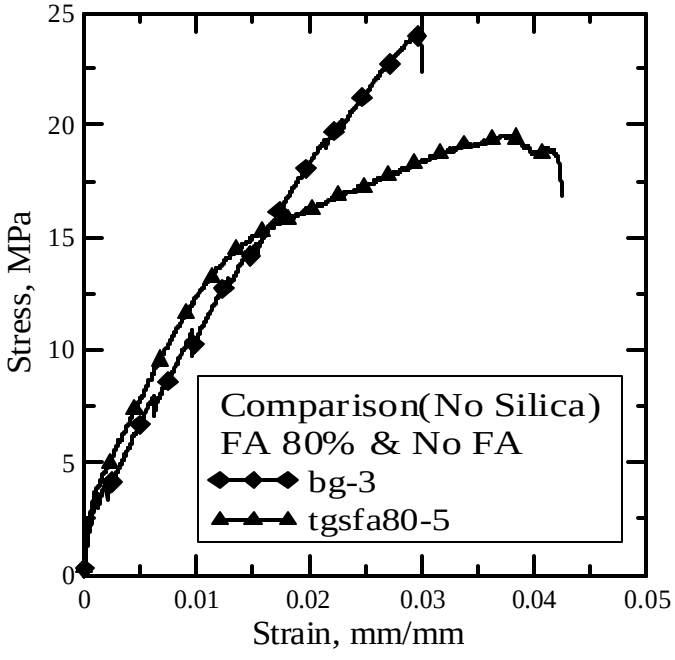

Fig. C-12. Comparison of AR-glass fiber samples with 80% FA and 0% FA (No SF)

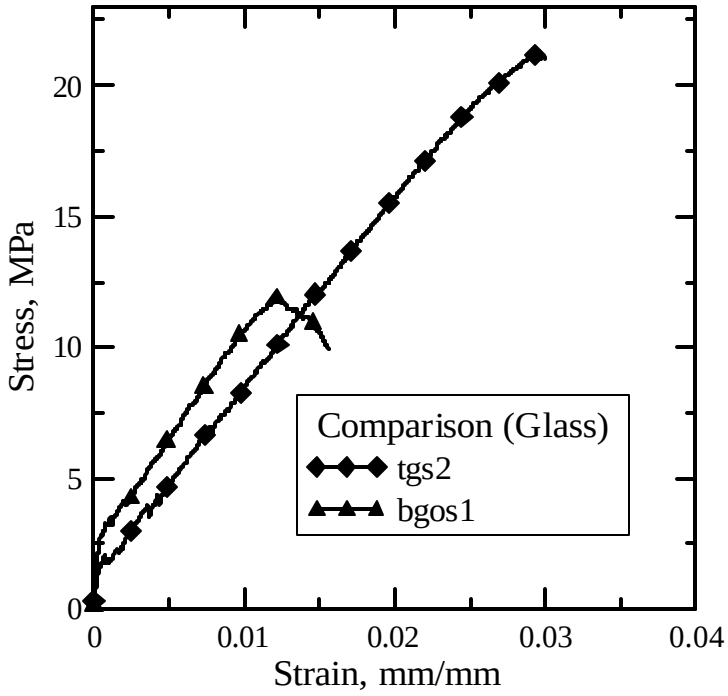

Fig. C-13. Comparison of AR-glass fiber samples with fabric in 0 and 90 orientations

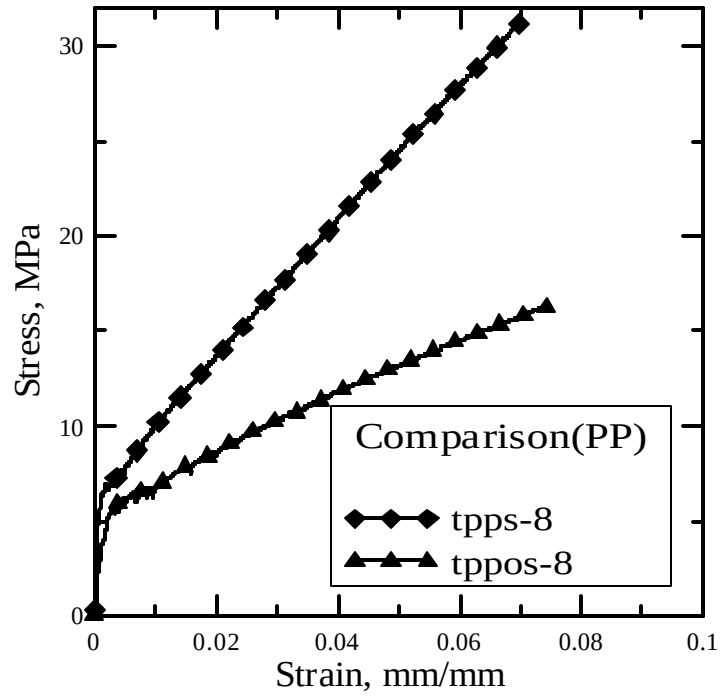

Fig. C-14. Comparison of PP fiber samples with fabric in 0 and 90 orientations